
FACULTAT DE QUÍMICA
DEPARTAMENT DE CIÈNCIA DELS MATERIALS I ENGINYERIA METAL·LÚRGICA

**Programa:** Tecnología de Materiales, bienio 2002-2004

# Recubrimientos biocompatibles obtenidos por Proyección Térmica y estudio *in vitro* de la función osteoblástica

Memoria presentada para optar al grado de Doctor en Ciencias Químicas por Mireia Gaona Latorre, bajo la dirección del Profesor Josep Maria Guilemany Casadamon y el Profesor Javier Fernández González

Barcelona, Junio 2007

# CAPÍTULO 8:

# Recubrimientos de titania nanoestructurada y titania nanoestructurada con hidroxiapatita mediante proyección térmica por alta velocidad

*¿Y no será que en este mundo hay cada vez más gente y menos personas?*

## 8.1 Introducción

Debido a los problemas de anclaje que presentan los recubrimientos de HA obtenidos por proyección térmica por la disolución preferencial de la fase amorfa (ACP) en medios fisiológicos, se requieren nuevas alternativas de recubrimientos para usos biomédicos con mejores prestaciones. Es obvio que si estos nuevos recubrimientos han de sustituir a los ya existentes de HA tendrían que tener entre las características principales: (i) no ser tóxicos ni reabsorbibles por el cuerpo humano,

(ii) tener un excelente funcionamiento mecánico y (iii) tener una buena interacción con las células osteoblásticas.

Durante décadas se ha utilizado satisfactoriamente el titanio como material para implantes. Se cree que la biocompatibilidad está relacionada con la interacción entre la capa superficial de óxido de titanio, que se forma espontáneamente, y el medio fisiológico. El óxido de titanio o titania es un material no tóxico, no reabsorbible y varios autores han demostrado que los recubrimientos de titania provocan una buena adsorción de iones de calcio y fosfato y de proteínas de los fluidos corporales que facilitan la adherencia celular [1, 2].

Del mismo modo, varios autores han demostrado que materiales nanoestructurados de alúmina ($Al_2O_3$), titania ($TiO_2$), HA, el titanio cp, y aleaciones de Ti-6Al-4V y Co28Cr6Mo presentan mejor biocompatibilidad con células osteoblásticas que sus análogos convencionales [3-6]. Esta mejor biocompatibilidad se refiere a una reproducción celular más elevada y a una mejor adherencia de las células sobre la superficie de estos materiales. Webster et al. [7], demostraron que estas mejoras del material nanoestructurado se debe al efecto de la nanotextura o nanorugosidad sobre la adsorción de las proteínas de adherencia, como la fibronectina, que tienen tamaños nanométricos. Estas proteínas de adherencia median la adherencia de células dependientes de anclaje sobre sustratos (como los osteoblastos) [8]. Éstas son adsorbidas sobre la superficie de un material casi inmediatamente después de su implantación en el cuerpo humano. Cuando las células osteoblásticas llegan a la superficie del implante se encuentran con una superficie cubierta por estas proteínas que se unirán con las proteínas transmembranas (integrinas).

Se ha demostrado que las proteínas nanométricas tiene mejor interacción o adsorción a una superficie nanotexturizada que a una microtexturizada [9]. Así mismo, Webster et al. [7] realizaron un estudio en el cual se colocaron diferentes proteínas

sobre la superficie de distintos sustratos que contenían regiones lisas y con algunas nanoprotuberancias. Durante este experimento se observó que las proteínas tendieron a interaccionar sobre las nanoprotuberancias, mientras que, no se observó ningún fenómeno significativo en las regiones lisas. Este fenómeno llevó a la conclusión que los materiales nanoestructurados podrían convertirse en una futura generación de materiales biomédicos.

Por otra parte, se ha observado que los recubrimientos nanoestructurados obtenidos por proyección térmica presentan mejores propiedades mecánicas que sus homólogos convencionales [10, 11]. Entre estas mejoras se encuentran una mayor resistencia al desgaste y a la delaminación, mejor adherencia al sustrato y una dureza y plasticidad más alta.

Por estos motivos se consideró que los recubrimientos nanoestructurados de titania podrían ser una alternativa interesante en prótesis no cementadas al tratarse, a priori, de un material no tóxico ni reabsorbible, tener una buena interacción con las células osteoblásticas y un excelente funcionamiento mecánico.

Para obtener este tipo de recubrimientos es necesario partir de polvo nanoestructurado. Existen dos problemas principales en el proceso de proyección de nanopartículas. El primero reside en que las partículas nanométricas, es decir de tamaño menor a 100 nm, no pueden ser proyectadas usando los alimentadores de polvo convencionales ya que podrían obstruir los conductos que las transportan del alimentador a la pistola. Una solución eficaz, sobretodo para partículas cerámicas, es aglomerar las partículas vía spray drying para obtener un tamaño micrométrico de polvo de proyección.

El otro problema deriva de que los procesos de proyección térmica están intrínsecamente asociados con la fusión total o parcial de las partículas proyectadas

para poder conseguir una adhesión y cohesión entre ellas. Si esta fusión no se produjese sería considerablemente difícil producir recubrimientos cerámicos. Esto es un inconveniente a la hora proyectar polvos nanoestructurados; ya que si las partículas se funden totalmente las características del polvo de partida desaparecerían y, consecuentemente, el recubrimiento no tendría ningún rasgo nanostructurado. Para evitar este problema es necesario tener un buen control de la temperatura de las partículas en el haz de proyección para mantenerla cerca del punto de fusión del material.

## 8.2 Objetivos

El trabajo que se muestra en este capítulo se realizó en colaboración con el Nacional Research Council of Canada (NRC). La colaboración se basó en la producción de recubrimientos nanoestructurados de titania ya que podrían ser una alternativa interesante a los de HA utilizados actualmente. Asimismo se realizaron mezclas de $TiO_2$ nanoestructurada y HA para dar a los recubrimientos las propiedades bioactivas de la HA. Cabe mencionar que de este último tipo de recubrimientos no hay referencias anteriores.

Los objetivos de este capítulo son:

- Obtención y caracterización de recubrimientos nanoestructurados de $TiO_2$ obtenidos mediante HVOF utilizando diferentes condiciones de proyección.

- Obtención y caracterización de recubrimientos nanoestructurados de $TiO_2$ con 10% y 20% de HA obtenidos mediante HVOF utilizando las mismas condiciones de proyección para evaluar el efecto de la HA en las propiedades del recubrimiento.

## 8.3 Resultados.

Los resultados obtenidos en este capítulo se muestran en los artículos:

- *The Influence of Particle Temperature and Velocity on the Microstructure, Mechanical Behaviour and Residual Stress Levels of High Velocity Oxy-Fuel (HVOF) Sprayed Nanostructured Titania Coatings*

- *Nanostructured titania/hydroxyapatite composite coatings deposited by high velocity oxy-fuel (HVOF) spraying*

## *The Influence of Particle Temperature and Velocity on the Microstructure, Mechanical Behaviour and Residual Stress Levels of High Velocity Oxy-Fuel (HVOF) Sprayed Nanostructured Titania Coatings*

M. Gaona, R. S. Lima, B. R. Marple

Journal of Materials Processing Technologies. Aceptado.

Resumen:

La titania es un material biocompatible por lo que en este trabajo se ha querido estudiar recubrimientos nanoestructurados como posibles candidatos para sustituir los de hidroxiapatita (HA) producidos industrialmente por proyección térmica de plasma atmosférico (APS).

En este trabajo se han estudiado tres recubrimientos de titania ($TiO_2$) nanoestructurada obtenidos mediante diferentes condiciones de proyección de HVOF. Los parámetros de proyección se ajustaron de manera que para un recubrimiento las temperaturas de las partículas fueran ligeramente inferiores a la temperatura de fusión de la titania, para otro ligeramente superior a la temperatura de fusión y , para el último de los tres recubrimientos, las partículas consiguieran la máxima temperatura de trabajo sin dañar la pistola de proyección.

Se estudió la microestructura, la porosidad, la rugosidad, la dureza y la adherencia del recubrimiento al substrato (ASTM C633) de este tipo de recubrimientos y presentaban propiedades mecánicas superiores a los de HA, menor porosidad, que actúa como barrera contra el desprendimiento de iones metálicos del substrato, y una baja rugosidad micrométrica. Además de esas características, la superficie de los recubrimientos presenta regiones nanotexturizadas que podrían mejorar la interacción con proteínas de adherencia de las células osteoblásticas, como vitronectina y fibronectina, a fin de favorecer la funcionalidad biológica del recubrimiento.

**The Influence of Particle Temperature and Velocity on the Microstructure, Mechanical Behaviour and Residual Stress Levels of High Velocity Oxy-Fuel (HVOF) Sprayed Nanostructured Titania Coatings**

M. Gaona [1], R. S. Lima [2,] * and B. R. Marple [2]

[1] Thermal Spray Centre
Universitat de Barcelona
Martí i Franquès 1
08028 Barcelona
Spain

[2] National Research Council of Canada
75 de Mortagne Blvd.
Boucherville, QC J4B 6Y4
Canada

*** Corresponding author**

Dr. Rogerio Lima
National Research Council of Canada
75 de Mortagne Blvd.
Boucherville, QC J4B 6Y4
Canada

e-mail: HTrogerio.lima@cnrc-nrc.gc.ca
Phone: +1-450-641-5150
Fax: +1-450-641-5105

2

**ABSTRACT**

Nanostructured titania feedstock powders were deposited via high velocity oxy-fuel (HVOF) spraying onto Ti-6Al-4V substrates. Using in-flight particle diagnostics, different particle temperatures and velocities were employed in order to reveal their effects on microstructure and mechanical properties of the coatings. It was observed a series of linear relationships involving particle temperature and velocity with microstructural features and coating properties, such as, residual stress levels, phase composition and Vickers hardness (300 gf). High bond strength values were observed when compared with other ceramic thermal spray coatings available in the literature. This study provides different levels of information on the processing of nanostructured ceramic powders via HVOF spraying and opens possibilities for development and application of HVOF-sprayed nanostructured titania coatings in the biomedical field and other disciplines, where superior mechanical behaviour is required.

**Keywords**: Thermal spray, high velocity oxy-fuel (HVOF), processing, in-flight particle diagnostics, nanostructured titania ($TiO_2$), microstructure, bond strength.

## 1. Introduction

### 1.1 Nanostructured Materials

Nanotechnology is an area that has offered many possibilities for turning fundamental research into successful progress. Nowadays, there is a lot of research in nanotechnologies involving medicine, electronics, materials science or other fields that are concerned with enhancing properties or producing new materials. The so-called conventional materials exhibit grain sizes ranging from several millimetres to microns, whereas, nanocrystalline materials are characterized by exhibiting grain sizes below 100 nm. Different studies reveal that, as the grain size decreases to nanostructured level, there is an important increase in grain boundaries that influences the chemical and physical properties of the material, which can differ substantially from those of the conventional materials [1]. For example, nanoceramic materials can exhibit improved mechanical properties and even superplasticity when compared to coarser-grained ceramics, as long as nanocrystalline ceramics can retain their grain sizes after sintering [2].

### 1.2 Biomedical Applications of Nanomaterials

Particularly, there is a considerable effort about the use of nanostructured materials in the biomedical field. It is widely accepted that the interaction between cells and biocompatible surfaces is essential to a wide range of disciplines, such as, tissue engineering, biotechnologies, implant materials and cell-based sensors [3, 4]. Different studies are focused on the possible use of nanostructured materials in prosthetic devices, since it is believed that they can be designed to have surfaces and mechanical properties similar to those of physiological bone. It has been reported that the materials that exhibit nanotextures on their surfaces will have an advantage in the interaction between the implant with the bone cells (e.g., osteoblasts) [5, 6]. It is hypothesized that the use of nanostructured coatings, containing regions on its surface exhibiting nanotexture (nanoroughness), could be an interesting method to improve the adhesion of the osteoblast cells on the coating surface, contributing for a better long term performance of the implant. It is believed that the nanotopography enhances the adsorption of extracellular matrix (ECM) adhesion proteins such as collagen, fibronectin, thrombospondin, vitronectin, and osteopontin, for cell integrin receptors [7]. These adhesion proteins are initially adsorbed on the prosthesis surface almost immediately upon its implantation in the human body. Cellular interactions with ECM molecules are supposed to produce specific signals that are transduced through the integrins to the cytoplasm, the cytoskeleton, and the nucleus of the osteoblasts [8]. Compared with conventional alumina and titania, osteoblast adhesion increased by 46% and 30% on nanophase 23-nm grain size alumina and on nanophase 32-nm grain size titania, respectively [9].

**1.3 Applications of Nanostructured Titania Thermally Sprayed Coatings**

Nanostructured titania thermally sprayed coatings have demonstrated excellent structural performance for anti-wear applications when compared to conventional titania coatings [10], mainly when the nanostructured feedstock powder is processed via high velocity oxy-fuel (HVOF) [11]. This type of anti-wear coating has been applied with success in high pressure acid leach hydrometallurgical processing equipment, which employs autoclaves, valves and piping in a severe high temperature acidic slurry environment [12].

Recently, the use of nanostructured titania thermally sprayed coatings in the biomedical field has also been cogitated [13-15]. Nowadays, there is a discussion about the stability of thermally sprayed hydroxyapatite (HA) coatings once implanted in vivo. Although the biocompatible and osteoconductive properties of HA coatings are well accepted [16], an important drawback comes from the instability of the substrate/coating interface and the unstable duration of coating in the presence of body fluids under local loading. For that reason the employment of a stable biocompatible and nanostructured coating materials, such as titania, could be a promising alternative to HA coatings on prosthetic devices.

Considering that, the aim of this work was to further study the HVOF processing of nanostructured titania powders, to produce coatings that combine enhanced mechanical performance with nanotexturization of their surfaces, envisioning biomedical applications.

**2. Experimental Procedure**

**2.1. Feedstock Powder, Thermal Spraying and Residual Stress**

Nanostructured titania ($TiO_2$) feedstock powder (VHP-DCS (5-20 μm)), Altair Nanomaterials Inc. Reno, NV, USA) was employed in this work. The particle size was measured by a laser Diffraction Particle Size Analyzer (Beckman Coulter LS 13320, Beckman Coulter, Miami, FL, USA) and the morphology was studied by means a Field Emission Scanning Electron Microscopy (FE-SEM) (S-4700, Hitachi, Tokyo, Japan). The feedstock powder was agglomerated and sintered and exhibited a nominal particle distribution from 5 to 20 μm, according to the powder manufacturer.

The powder was thermally sprayed onto previously grit-blasted Ti-6Al-4V substrates by using an oxygen-propylene HVOF torch (Diamond Jet 2700-hybrid, Sulzer Metco, Westbury, NY, USA). Particle diagnostics (temperature and velocity) was carried out based on an in-flight diagnostic tool (DPV 2000, Tecnar Automation, Saint Bruno, QC, Canada). This diagnostic system is based on optical pyrometry and time-of-flight measurements that allows on-line measurements of the distributions of particle temperature, velocity and diameter in the spray jet. A total of 5000 particles were measured at the centreline of the spray jet, where the particle flow was the highest, for

each one of the three spray condition employed in this work. The particle detector was placed at the same spray distance as used when depositing the coatings (Table 1).

Considering the spray parameters, based on previous experience, the oxygen and air flows of the HVOF torch were kept constant at 279 and 202 litres per minute (lpm) and the propylene flow was varied. After a series of tests that involved variations of propylene flow, three sets of spray parameters were chosen. Two sets that exhibited average particle temperature levels approximately 20ºC above and below the melting point of titania (1855ºC) [17], and the third set that exhibited the highest particle temperature and velocity without causing damage to the spray torch by excessive heat of the flame. The powder feed rate and the carrier gas ($N_2$) flow were kept constant at 10 g/min and 54 lpm, respectively. The spraying parameters employed are summarized in Table 1. A statistical software (StatGraphics Plus 2.0, Statistical Graphics, Rockville, MD, USA) was employed to determine the correlations among the spray parameters, in-flight particle characteristics and microstructural features.

During the spraying process a cooling system (air jets) was applied to reduce the coating temperature, which was monitored using a pyrometer. The maximum surface temperatures for the coatings were approximately 130$^{o}$C, 160$^{o}$C and 250$^{o}$C for the propylene flows of 65 lpm, 70 lpm and 90 lpm, respectively (Table 1).

Coatings were evaluated for residual stress by Almen strips (type, N; grade I) (Electronics Inc., Mishawaka, IN, USA), that were mounted alongside the substrates and coated during the spraying process. The arc height (deflection) on the Almen strip was measured after grit blasting the surface (first reading) and again after coating application (second reading). The deflections of the Almen strips were read via an Almen gauge (Model TSP-3, Electronics Inc., Mishawaka, IN, USA), and reported as the difference of the two readings, second reading minus the first reading. Positive or negative deflection values were considered to represent tensile or compressive residuals stress levels, respectfully. The absence of Almen deflection was considered as non-significant or neutral stress levels.

**2.2 Coating Microstructure, Porosity and Phase Characterization**

The cross-sections of the coatings were examined by means of an FE-SEM. For the observation of the cross-section and determination of the coating porosity, the samples were cut, vacuum impregnated with a low viscosity epoxy resin and polished up to 4 μm alumina emulsion. Vacuum impregnation was used to differentiate porosity, gaps, cracks and loose particles that can easily be altered or even removed during metallographic preparation. Digital image analysis was used to determine the porosity by the observation of the polished cross-section of the coatings discerning the original pores are embedded by resin to the pores formed during the metallographic preparation in order to discern both types of pores. A total of 10 images per coating were analyzed to determine the porosity levels.

X-ray diffraction (XRD; Cu Kα radiation) was used to determine the phases present in the coatings and feedstock powder. A 2θ diffraction angle ranging from 20-60$^{o}$ (using a step size of 0.05$^{o}$ and step time of 2.5 s) was employed.

**2.3 Microhardness and Bond Strength**

Microhardness values of the coatings were measured using a Vickers microhardness tester with indentation loads of 300gf for 15s. A total of 10 microhardness measurements were performed for each coating. The ASTM standard C633-01 [18] was carried out to determine the degree of adhesion or bonding strength of the coatings to the substrates or the cohesion strength of the coating in a tension normal to the surface. The loading rods were grit-blasted and attached to the surfaces of the coatings using a special adhesive-bonding tape (FM 1000, American Cyanamid, Wayne, NJ, USA). Both roads were then joined using compressive stress while curing at 203ºC for 3 hours in an oven. The pressure of the roads is then released and the resin-bonded rods were pulled out using a universal tension testing machine and a load at a rate 1 of mm/min. Five samples were tested for each spraying condition and the average value is reported.

**3. Results and Discussion**

**3.1 Nanostructured Titania Feedstock Powder**

A typical morphological structure of the spray dried powders is shown in Fig. 1. The nanostructured titania feedstock Altair VHP-DCS (5–20 μm), was agglomerated and sintered. It exhibits the typical donut-shape of spray-dried particles. When the powder is analyzed at high magnifications (Fig. 1b), it is possible to observe an agglomeration of titania nanoparticles smaller than 100 nm. Based on the results of Fig. 2, it is possible to observe that the majority of the spray-dried agglomerates exhibited diameters varying from 5 to 20 μm

**3.2 In-Flight Particle Characteristics**

In-flight particle diagnostics was performed in order to relate changes in the coating properties to changes in the in-flight particle temperature and velocity characteristics. Table 1 summarizes the average particle temperature and velocity for each spraying condition, whereas, Fig. 3 shows the particle temperature and velocity distributions in the thermal spray jet. The histograms show distributions that shift to higher particle temperature and velocity values as the propylene flow increases. The effect of propylene flow rate is significant and noteworthy. As the propylene flow increases, more particles exhibited temperatures at their surfaces above the melting point of titania (1855$^{o}$C [17]) and an increase on particle velocity was observed.

During the HVOF spray processing, the powder particles are heated and accelerated at high speeds by the combustible gases. The maximum particle temperature and velocity was obtained with fuel-richest conditions. It is important to point out that a strong linear dependence has been found to relate the propylene flow with the particle temperature (Fig. 4) and velocity (Fig. 5), when the oxygen and air flow were kept constant at 279 lpm and 202 lpm, respectfully. From the results of Figs. 4 and 5, the following relationships can be derived between the propylene flow and particle temperature and velocity:

$$T\ (^{o}C) = 1226.33 + 9.4 \times \text{propylene flow (lpm)} \quad \text{Eq. 1}$$

$$V\ (m/s) = 105.429 + 8.3 \times \text{propylene flow (lpm)} \quad \text{Eq. 2}$$

This linear relationship between particle temperature and velocity in HVOF spraying of this powder is evident by looking at Fig. 6. It is important to point out that these linear trends between particle and temperature were also observed for the HVOF spraying of multimodal and conventional WC-Co powders, for different torches and spray parameters, using fuels like propylene, hydrogen and kerosene [19]. Therefore it is inferred that this is a typical behaviour of HVOF processing, when the particle detector is placed at the same spray distance as used when depositing the coatings.

**3.3 Microstructural Characterization**

The SEM images of the cross-section microstructures of the coatings can be observed in Fig. 7. Thermal spray coatings are known for their lamellar microstructure [20], but in this case for the HVOF-sprayed nanostructured titania coatings, the traditional splat structure of the thermal sprayed coatings was not observed. When analyzing the cross-section of the coating HVOF-sprayed produced at 90 lpm of propylene, it can be stated that this coating exhibited an isotropic-like microstructure, with characteristics very similar to those of "bulk" materials.

The relationship involving average particle temperature and velocity with porosity can be observed at Fig. 8. Coating porosity decreases with increasing particle temperature and velocity values, which both equally affect the porosity levels, in the same mode and intensity. The measured porosity is below 1% for average particle temperature and velocity levels at 2073 ± 141ºC and 854 ± 112 m/s, respectively. The porosity values obtained for the other two sets of spray parameters are similar or lower than those for coatings produced via air plasma spray (APS), due to the higher kinetic energy levels imparted by HVOF torches to the sprayed particles [21, 22].

Some authors [23, 24] proposed porous structures and large interconnected pores that support cell attachment, which are progressively filled with mature new bone tissue. These porous structures would tend to provide enhanced osteointegration in implants. However, near pore-free coatings, such at that of Fig. 7c, may protect metallic prosthesis from environmental attack and reducing the possible release of ions from the underlying implant. In addition, it was reported that

the nano-sized surface textures will exhibit an advantage in the interaction between the implant with the bone cells. It was shown that the nanotopographies of different materials enhance the adsorption of extracellular matrix (ECM) adhesion proteins that interact with osteoblast cells [5, 6].

An example of nanotexture on the surface of these HVOF-sprayed nanostructured titania coatings is shown in Fig. 9 [25], which is the result of a semi-molten particle (like that of Fig. 1) that was deposited on the surface of the coating.

**3.4 Residual Stress**

Almen strips were used to compare the effect of the different particle temperature and velocity levels on the residual stresses. By looking at Fig. 10 it is possible to observe that there is a strong linear relationship between average particle temperature and velocity with the deflection of the Almen strip. Despite this linear relationship, it is important to point out that Almen strips provide a qualitative value of residual stress, therefore, there is not necessarily a linear relationship involving particle temperature and velocity with residual stress levels. At the lowest particle temperature and velocity values, it was possible to produce a coating without significant levels of residual stress, however, for coatings produced under higher values of particle temperature and velocity, it was clearly observed that they exhibited compressive residual stress levels, i.e., negative values of Almen strip deflection. Compressive residual stress plays an important role with respect to the operating performance of the coatings. It may restrain crack propagation all through the coating and has a beneficial effect on the fatigue life [26], however, excessive compressive stress levels may lower the bond strength of the coating.

These compressive residual stress levels originated during HVOF spraying are considered to be generated by different factors. One of the most important ones is caused by the impinging molten and semi-molten particles at the high HVOF speeds, creating a peening effect, generating compressive stresses that may extend to a great depth into the substrate [27]. Therefore, the higher the particle velocity, the higher the compressive residual stress, as observed in Fig. 10.

Moreover, according to Stokes et al. [28], during the coating deposition when molten or semi-molten sprayed particles impinge onto a surface, the particles shrink due to quenching and a compressive residual stress is created as the coating is built up. It can be hypothesized that when the particles are sprayed at higher velocities and temperatures, (i) the higher velocities would improve intersplat contact (reducing porosity – Figs. 7 and 8), enhancing heat transfer from the re-solidifying particle to the coating, (ii) which in addition to the higher particles temperatures, would maximize quenching effects, thereby also maximizing residual stress levels.

**3.5 Phase Composition**

Figure 11 shows the XRD patterns of the nanostructured feedstock and coatings. Only rutile and anatase phases were detected in all samples. Rutile is the stable phase of the three polymorphic forms of titania at atmospheric pressure, whereas anatase and brokite are metastable and transform irreversibly to rutile at the range of 400-1000ºC [17]. The starting temperature of the anatase-rutile transformation depends on the microstructure of the powders of anatase, as well as, on the size of the particles and other microstructural parameters.

Figure 12 shows the effect of average particle temperature and velocity on the anatase content in the coatings. The volume percentage of anatase (in volume) was determined according to the following Eq. 3 [29]:

$$C_A = \frac{8I_A}{(13I_R + 8I_A)} \qquad \text{(Eq. 3)}$$

where $I_A$ and $I_R$ are the X-ray intensities of the anatase (1 0 1) and the rutile (1 1 0) peaks, respectively. Anatase was the predominantly phase in the original feedstock. However, after HVOF spraying, the major phase was rutile and the minor phase was anatase. By looking at Fig. 12 it is possible to observe a relatively strong linear relationship involving particle temperature and velocity with the content of anatase in the coatings. It is possible to observe that higher values of particle temperature and velocity induced higher contents of anatase (the major feedstock phase) in the coating microstructure.

The anatase phase found in these coatings was probably the result of semi-molten feedstock particles that became embedded in the coating microstructure after thermal spraying. An example of an embedded semi-molten particle is found in Fig. 13. It is important to point out that the temperatures of the particles measured in this study (via pyrometry) are surface temperatures. The maximum temperature of a propylene flame of the HVOF torch is below 3,000$^{o}$C. These maximum temperature levels are much lower than those of plasma spray jets, which may reach 15,000$^{o}$C [30].

By looking at Fig. 2, it can be observed that for a 90 lpm flow of propylene, the majority of the sprayed particles exhibited “surface” temperatures higher than that of the melting point of titania, which is 1855$^{o}$C [17]. From the results of Fig. 2, one can conclude that not only the smaller but also the larger particles from the powder distribution (Fig. 2) were successfully deposited on the substrate surface. Due to the relatively low temperatures of the HVOF flame (compared to those of APS), it is hypothesized that a fraction of the larger particles of the feedstock was not fully molten during their dwell time in the HVOF flame, i.e., the inner core of these particles exhibited temperatures below that of the melting point of titania. These non-molten cores (particles), became deposited on the coating surface and embedded in the coating microstructure (as shown in Figs. 9 and 13) and responsible for the detection of higher contents of anatase phase for higher particle temperature and velocity values (Fig. 12). It is important to highlight that higher amounts of anatase phase for APS titania coatings were observed when plasma spraying was carried out at lower powder levels,

employing plasma gas mixtures that resulted in lower thermal conductivities. Berger-Keller et al [29] also attributed to semi-molten titania particles the higher anatase content of those coatings. Finally, due to the high particle velocities and short spray distances employed in this work (Table 1), it is estimated that the non-molten cores would be subject to high temperatures for milliseconds, which would probably impede solid phase transformation from anatase to rutile.

**3.6 Hardness and Bond Strength**

The relationship involving average particle temperature and velocity with Vickers hardness numbers (300 gf) can be observed at Fig. 14. It is possible to observe a relatively strong linear relationship involving particle temperature and velocity with the hardness values of the coatings. Higher particle temperatures and velocities enhance the intersplat contact, thereby increasing the cohesive strength of the coating. It is important to point out that the range of hardness numbers varied from ~700 to ~900 (Fig. 14). These values are higher than those reported for bulk HA samples, which were sintered at the temperature range of 1250-1350$^{o}$C. The higher Vickers hardness number (300 gf) obtained was 513 ± 52 [31]. Therefore, these HVOF-sprayed nanostructured titania coatings exhibit cohesive strength levels higher than those of bulk HA.

It should be highlighted that Vickers hardness values were more affected by the in-flight variations of particle characteristics than the bond strength values, i.e., all nanostructured titania coatings failed at the epoxy glue during bond strength testing (ASTM C633-01) [18]. Because these samples exhibited glue failure, the exact bond strength of these coatings could not be quantified. The strength of the epoxy glue was previously tested and indicated a value of 77 MPa (~11,000 psi), therefore, the bond strength values of all nanostructured titania coatings produced in this study were higher than this value. It was already observed that HVOF-sprayed nanostructured titania coatings exhibit high bond strength values when deposited on low carbon steel substrates (56 MPa - ~8,000 psi) [11].

The higher bond strength of the nanostructured coatings was explained by this higher interfacial toughness observed by Bansal et al. for APS nanostructured ceramic coatings [32]. For conventional ceramic coatings it was observed that the interfaces between the particles that were fully molten in the spray jet and the steel substrate exhibited microcracks. For the nanostructured coating it was observed that the interfaces between the particles that were semi-molten in the thermal spray jet (i.e., dense nanozones – like that of Fig. 13) and the steel substrate were adherent, i.e., no microcracks or gaps. Therefore an interfacial crack in the nanostructured coating would tend to be interrupted by the strong adherent dense nanozones, thereby increasing interfacial toughness and bond strength. In addition to this mechanism and the typical mechanical anchoring of the thermally sprayed splats on the grit-blasted substrate surface, a chemical reaction between the oxidized surface of the Ti-based substrate probably occurred with the titania particles, thereby enhancing the coating bond strength.

Although thermally sprayed HA coatings possess excellent biological and osteoconductive properties, the bond strength values of these coatings on Ti-6Al-4V substrates are lower than the values achieved for other bioceramic coatings. The bond strength of the hydroxyapatite HVOF and APS coatings, generally exhibits bond strengths values generally below 31 MPa [33]. Therefore, the bond strength values of HVOF-sprayed coatings produced from nanostructured titania powders surpassed those of HA thermally sprayed coatings. This is a very important characteristic when selecting a biomedical coating.

**4. Conclusions**

During this work HVOF-sprayed nanostructured titania coatings were produced with different spraying conditions, in order to correlate particle temperature and velocity with the coating microstructure and properties, which will help to engineer future nanostructured and conventional ceramic coatings for different applications. The following conclusions were observed:

- There is a strong linear relationship between particle temperature and particle velocity when spraying this type of powder using HVOF-spraying.

- Despite not showing a liner relationship, the average particle temperature and velocity values equally affect the porosity levels of the coatings, in the same mode and intensity.

- There is a strong linear relationship involving average particle temperature and particle velocity with the deflection of Almen strips for these HVOF-sprayed coatings. The higher average particle temperatures and velocities induce higher compressive stress levels. These residual stress levels were probably caused by (i) the impinging molten and semi-molten particles at the high HVOF speeds, creating a peening effect and (ii) by the quenching and shrinking of molten and semi-molten sprayed particles on the surface, which generates compressive residual stress as the coating is built up.

- The major phase of the nanostructured feedstock powder is anatase, whereas the major phase of the HVOF-sprayed coatings is rutile. It was observed a relatively strong linear relationship involving particle temperature and velocity with the content of anatase in the coatings. The higher the average particle temperature and velocity, the higher the content of the anatase phase. It is hypothesized that semi-molten feedstock particles embedded in the coating microstructure are the responsible for the presence of the minor anatase phase in the coating.

- It was observed a relatively strong linear relationship involving particle temperature and velocity with the Vickers hardness numbers (300 gf) of the coatings. The higher the average particle temperature and velocity, the higher the Vickers hardness number. Higher particle temperatures and velocities enhance the intersplat contact, thereby increasing the cohesive strength of the coating. The Vickers hardness numbers (300 gf) obtained for the coatings were higher than that of the bulk HA.

- The bond strength values of all coatings were higher than 77 MPa (~11,000 psi) on Ti-6Al-4V substrates, which are higher than those reported for thermally sprayed HA coatings.

- It is hypothesised that the presence of semi-molten nanostructured particles in the coating surface (nanotexture) can have an important role in cell adhesion if these coatings are to be used in biomedical applications.

**Acknowledgements**

The authors thank J-F. Alarie for metallography and adhesion testing, F. Belval for HVOF spraying, M. Lamontagne for in-flight particle diagnostics and M. Thibodeau for SEM observations. Moreover, M. Gaona thanks the Generalitat de Catalunya (Spain) for the Formació de Personal Investigador (FI) grant and the Thermal Spray Centre for the financial support.

**References**

[1] S.C. Tjong, H. Chen, Nanocrystalline materials and coatings, Mater. Sci. Eng. R. 45 (2004) 1-88.

[2] F. Wakai, N. Kondo, Y. Shinoda, Ceramics superplasticity. Curr. Opinos Solid State Mater. Sci, 4 (1999) 461–465.

[3] D.G. Castner, B.D. Ratner, Biomedical surface science: Foundations to frontiers, Surf. Sci., 500(1-3) (2002) 28-60.

[4] B. Kasemo. Biological surface science. Surf. Sci., 500 (1-3) (2002) 656-677.

[5] L.G. Gutwein, T.J. Webster, Increased viable osteoblast density in the presence of nanophase compared to conventional alumina and titania particles, Biomaterials 25 (2004) 4175-4183.

[6] T.J. Webster, C. Ergun, R.H. Doremus, R.W. Siegel, R. Bizios, Enhanced functions of osteoblasts on nanophase ceramics, Biomaterials, 21(17) (2000) 1803-1810.

[7] V. Petit, J.P. Thiery, Focal adhesions: structure and dynamics, Biol. Cell., 92(7) (2000) 477-494.

[8] I. Degasne, M.F. Baslé, V. Demais, G. Huré, M. Lesourd, B. Grolleau, L. Mercier, D. Chappard, Effects of Roughness, Fibronectin and Vitronectin on Attachment, Spreading, and Proliferation of Human Osteoblast-Like Cells (Saos-2) on Titanium Surfaces, Calcif. Tissue Int., 64 (1999) 499-507.

[9] T.J. Webster, R.W. Siegel, R. Bizios, Osteoblast Adhesion on Nanophase Ceramics, Biomaterials, 20 (1999) 1221-1127.

[10] G.E. Kim, J. Walker Jr., J. B. Williams Jr., Nanostructured Titania Coated Titanium, US Patent 6,835,449 B2, December 28, 2004.

[11] R.S. Lima, B. R. Marple, From APS to HVOF spraying of conventional and nanostructured titania feedstock powders: a study on the enhancement of the mechanical properties, Surf. Coat. Technol., 200 (2006) 3428-3437.

[12] G. E. Kim, Proven and Promising Applications Thermal Sprayed Nanostructured Coatings, PDF file in Proceedings of the International Thermal Spray Conference 2006, PDF file in Building on 100 Years of Success: Proceedings of the International Thermal Spray Conference 2006, B. R. Marple, M. M. Hyland, Y–C. Lau, R. S. Lima, and J. Voyer, Eds., May 15-18, 2006 (Seattle, WA, USA), ASM International, Materials Park, OH, USA, 2006.

[13] X. Liu, X. Zhao, R.K.Y. Fu, J.P.Y. Ho, C. Ding, P.K. Chu, Plasma-Treated Nanostructured $TiO_2$ Surface Supporting Biomimetic Growth of Apatite, Biomaterials, 26 (2005) 6143-6150.

[14] X. Zhao, X. Liu, C. Ding, P. K. Chu, In Vitro Bioactivity of Plasma-Sprayed $TiO_2$ Coatings after Sodium Hydroxide Treatment, Surf. Coat. Technol., 200 (2006) 5487-5492.

[15] J.G. Legoux, F. Chellat, R.S. Lima, B.R. Marple, M.N. Bureau, H. Shen, G.A. Candeliere, Development of osteoblast colonies on new bioactive surfaces, J. Thermal Spray Technol., 15(4) (2006) 628-633.

[16] T.W. Bauer, R.C.T. Geesink, R. Zimmerman, J.T. McMahon, Hydroxyapatite-coated femoral stems - histological analysis of components retrieved at autopsy, J. Bone Joint Surg. Am. 73A (10) (1991) 1439-1452.

[17] M. Miyayama, K. Koumoto, and H. Yanagida: "Engineering Properties of Single Oxides" in Engineered Materials Handbook, 4- Ceramic and Glasses, S.J. Schneider, ed., ASM International, Materials Park, OH, USA, 1991, 748-757.

[18] Standard test method for adhesion or cohesion strength of thermal spray coatings, Annual Book of ASTM Standard C633-01, ASTM, West Conshohocken, PA, USA.

[19] B.R. Marple, R.S. Lima, Process temperature/velocity-hardness-wear relationships for high-velocity oxyfuel sprayed nanostructured and conventional cermet coatings, J. Thermal Spray Technol., 14(1) (2005) 67-76.

[20] L. Pawlowski, The Science and Engineering of Thermal Spray Coatings, Wiley, West Sussex, England, 1995.

[21] P. Ctibor, P. Boháč, M. Stranyánek, R. Čtvrtlík, Structure and mechanical properties of plasma sprayed coatings of titania and alumina, J. Eur. Ceram. Soc., In Press, Corrected Proof.

[22] H. Du, J.H. Shin, S.W. Lee, Study on Porosity of Plasma-Sprayed Coatings by Digital Image Analysis Method, J. Therm. Spray Technol., 14(4) 2005 453-461.

[23] P.S. Eggli, W. Muller, R.K. Schenk, Porous hydroxyapatite and tricalcium phosphate cylinders with two different pore size ranges implanted in the cancellous bone of rabbits. A comparative histomorphometric and histologic study of bony ingrowth and implant substitution, Clin. Orthop. Relat. Res., 232 (1998) 127-138.

[24] B.S. Chang, C.K. Lee, K.S. Hong, H.J. Youn, H.S. Ryu, S.S. Chung, K.W. Park, Osteoconduction at porous hydroxyapatite with various pore configurations, Biomaterials, 21(12) (2000) 1291-1298.

[25] R.S. Lima, B.R. Marple, Thermal spray coatings engineered from nanostructured ceramic agglomerated powders for structural, thermal barrier and biomedical applications: a review, J. Therm. Spray Technol., 16(1) (2007) 1-24.

[26] R.T.R. McGrann, D.J. Greving, J.R. Shadley, E.F. Rybicki, B.E. Bodger, D.A. Somerville, The effect of residual stress in HVOF tungsten carbide coatings on the fatigue life in bending of thermal spray coated aluminium, J. Therm. Spray Technol., 7(4) (1998) 546-552.

[27] P. Bansal, P.H. Shipway, S.B. Leen, Effect of particle impact on residual stress development in HVOF sprayed coatings, J. Therm. Spray Technol., 15(4) (2006) 570-575.

[28] J. Stokes, L. Looney, HVOF system definition to maximise the thickness of formed components, Surf. Coat. Technol., 148(1) (2001) 18-24.

[29] N. Berger-Keller, G. Bertrand, C. Filiatre, C. Meunier, C. Coddet, Microstructure of plasma-sprayed titania coatings deposited from spray-dried powder. Surf. Coat Technol., 168(2) 2003 281–290.

[30] E. Pfender, Fundamental studies associated with the plasma spray process, Surf. Coat. Technol., 34 (1988) 1-14.

[31] M.A. Lopes, F.J. Monteiro, J.D. Santos, Glass-reinforced composites: fracture toughness and hardness dependence on microstructural characteristics, Biomaterials, 20 (1999) 2085-2090.

15

[32] P. Bansal, N.P. Padture, A. Vasiliev, Improved Interfacial Mechanical Properties of $Al_2O_3$-13wt% $TiO_2$ Plasma-Sprayed Coatings Derived from Nanocrystalline Powders, Acta Mater., 51 (2003) 2959-2970.

[33] H. Li, KA. Khor, P. Cheang, Effect of the Powders' Melting State on the Properties of HVOF Sprayed Hydroxyapatite Coatings, Mat. Sci. Eng. A, 293 (2000) 71-80.

16

Tables:

Table **¡Error! Sólo el documento principal.** - HVOF spray parameters and average particle temperature and velocity for each set (oxygen flow: 279 lpm – air flow: 202 lpm)

| **Propylene flow (lpm)** | **Spray distance (cm)** | **T ($^{o}$C)** | **V (m/s)** |
|---|---|---|---|
| 65 | 20 | 1840 ±150 | 647 ±86 |
| 70 | 20 | 1881 ±162 | 686 ± 93 |
| 90 | 18 | 2073 ±141 | 854 ±112 |

17

Figures:


(a)

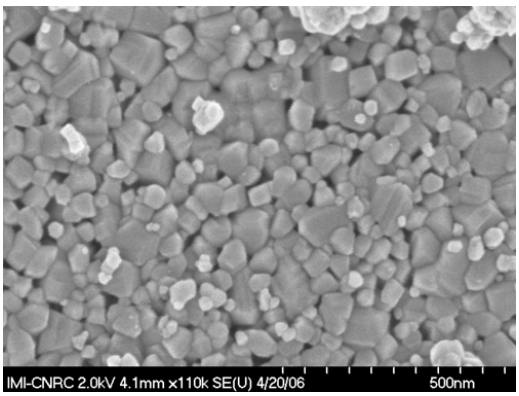


(b)

Figure 1 - a) Typical morphology of agglomerated spray-dried titania powders. b) High magnification view of (a) - agglomeration of individual nanosized titania particles.

18

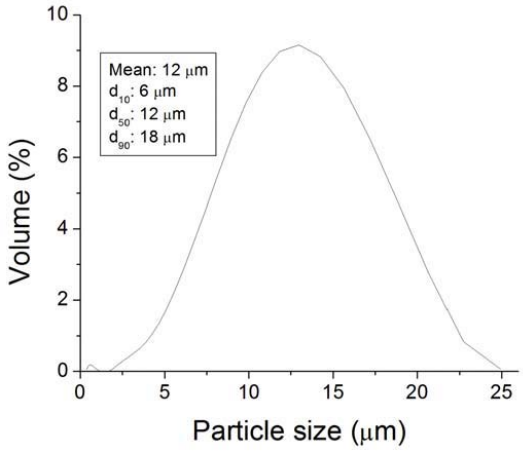


Figure 2 – Size distribution of the spray-dried nanostructured titania agglomerates.

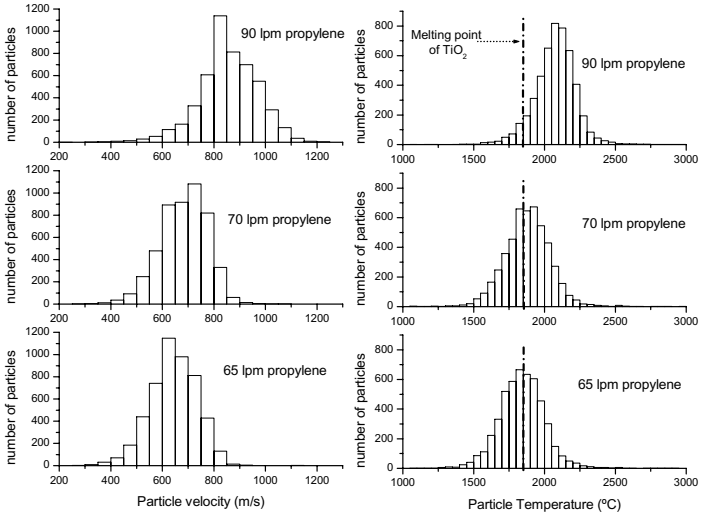


**Figure 3 - Histograms of the particle velocity and temperature (n = 5000).**

19

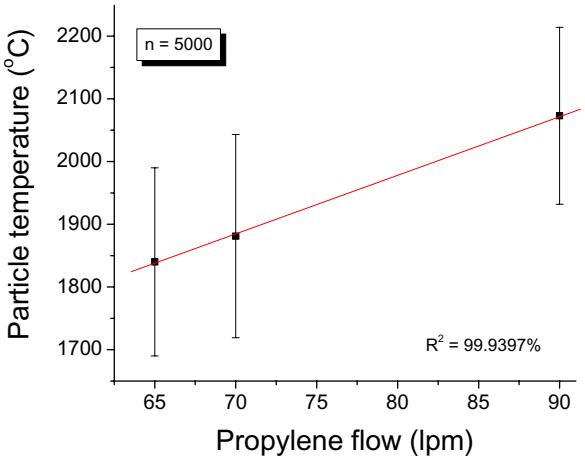


Figure 4 – Relationship between the propylene flow and particle temperature.

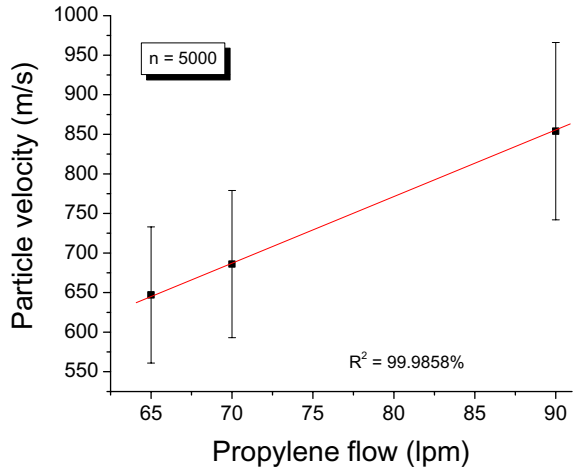


Figure 5 – Relationship between the propylene flow and particle velocity.

20

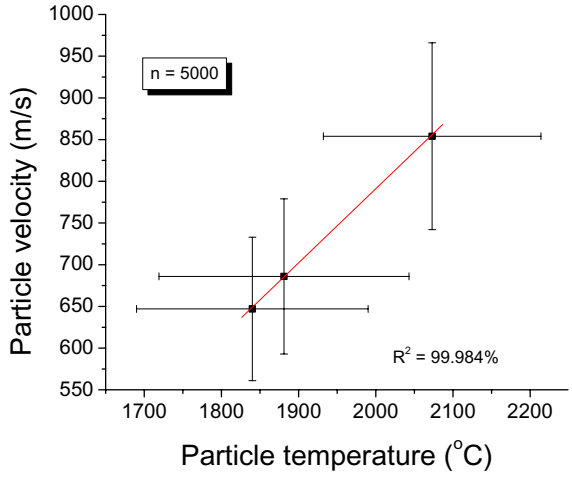


Figure 6 – Relationship between particle temperature and particle velocity.

21

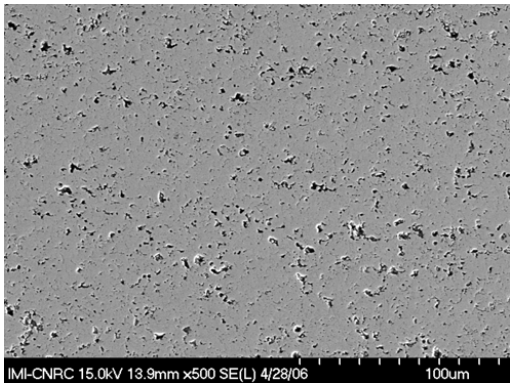


(a)

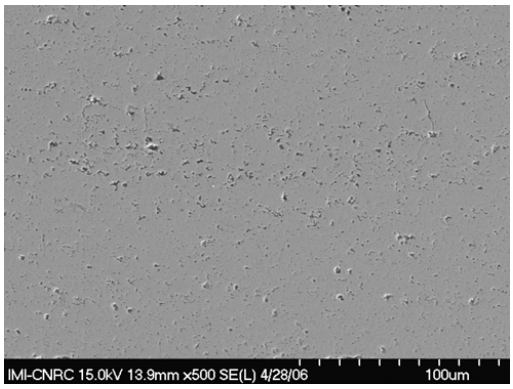


(b)

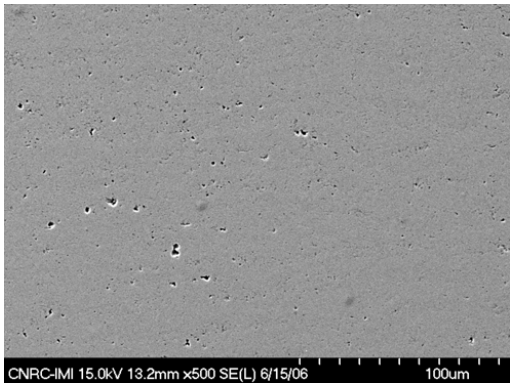


(c)

Figure 7 - SEM cross-section images of the different coatings. (a) 65 lpm propylene, (b) 70 lpm propylene, (c) 90 lpm propylene.

22

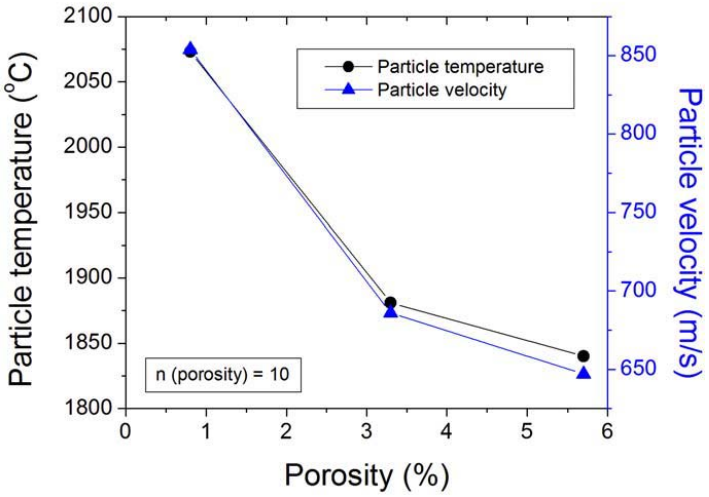


Figure 8 – Combined effect of average particle temperature and velocity on the porosity levels of the HVOF-sprayed nanostructured titania coatings.

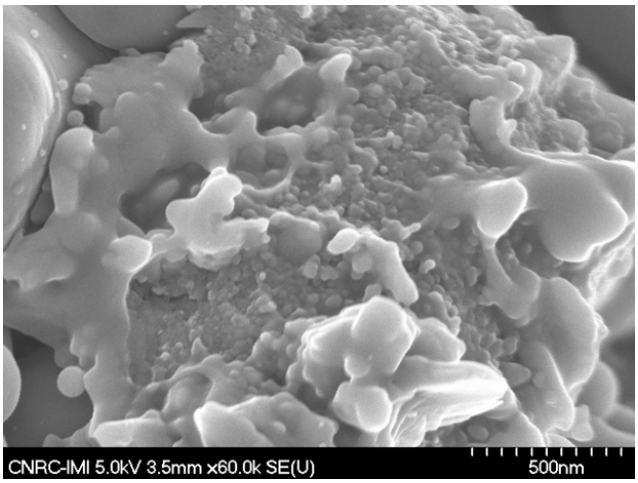


Figure 9 – Nanotexture formed by a semi-molten agglomerate on the surface of an HVOF-sprayed nanostructured titania coating [25].

23

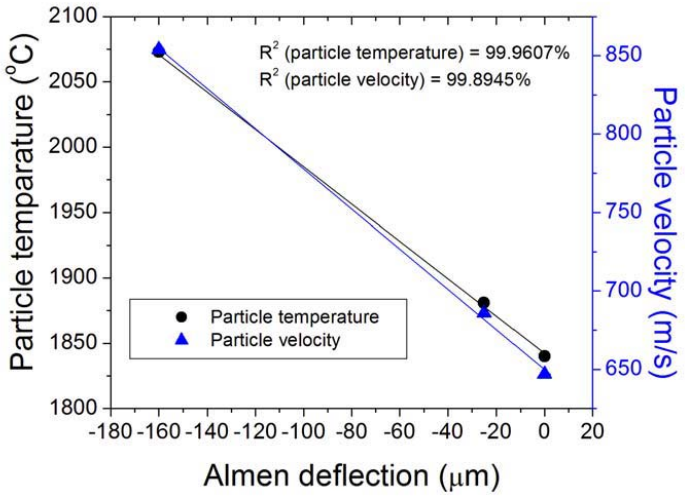


Figure 10 – Combined effect of average particle temperature and velocity on the residual stress levels of the HVOF-sprayed nanostructured titania coatings.

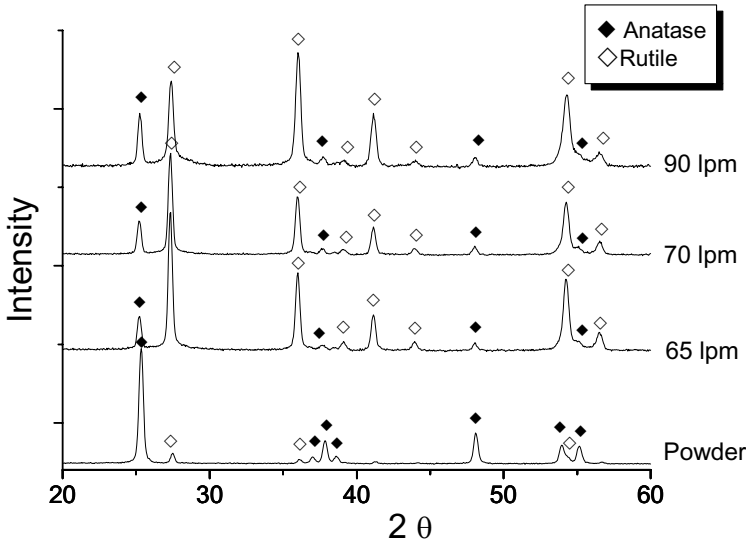


Figure 11 - XRD patterns of the feedstock and the HVOF nanostructured titania coatings.

24

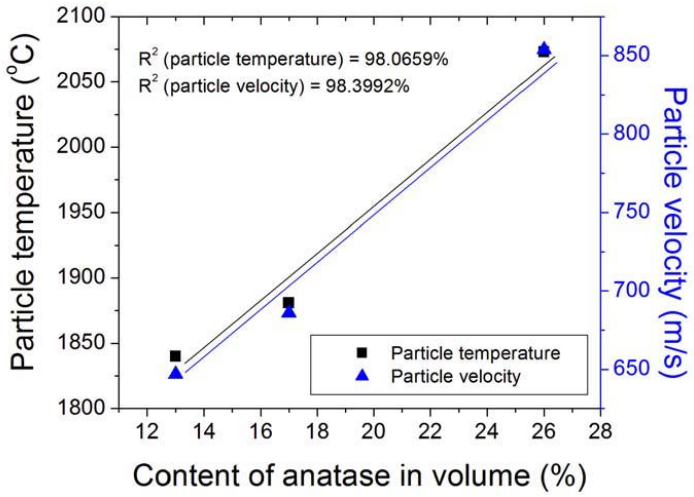


Figure 12 – Combined effect of average particle temperature and velocity on the anatase content levels of the HVOF-sprayed nanostructured titania coatings.

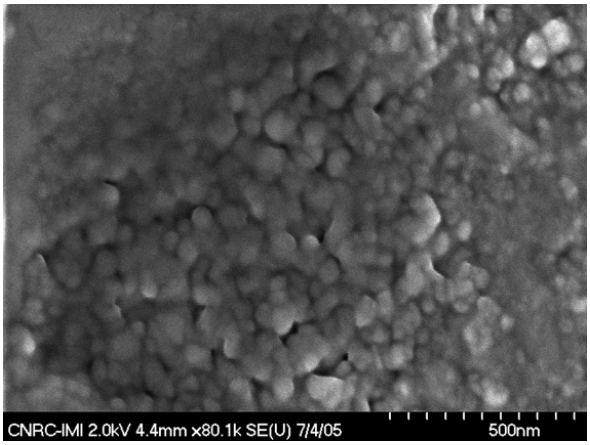


Figure 13 – High magnification view of an HVOF-sprayed titania coating showing a semi-molten particle (as that of Fig. 1), embedded in the coating microstructure [25].

25

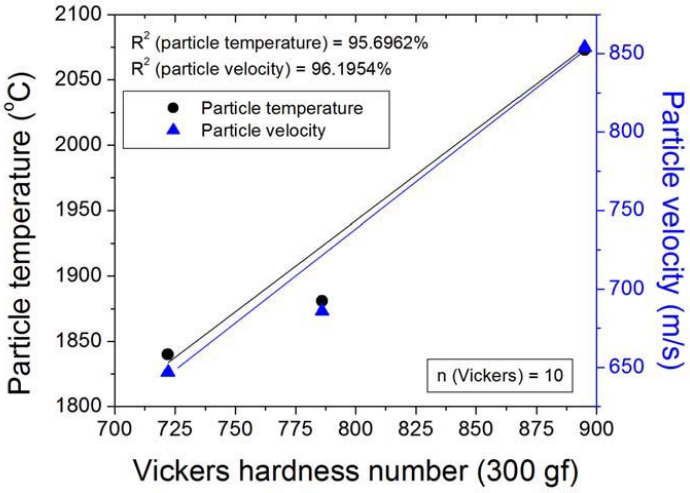


Figure 14 – Combined effect of average particle temperature and velocity on the Vickers hardness numbers (300 gf) of the HVOF-sprayed nanostructured titania coatings.

## *Nanostructured titania/hydroxyapatite composite coatings deposited by high velocity oxy-fuel (HVOF) spraying*

M. Gaona, R. S. Lima, B. R. Marple

Materials Science and Engineering A. 458, (2007), 141–149

Resumen:

En este trabajo polvo de titania puro y mezclado con un 10% y un 20% de HA fue proyectado por alta velocidad (HVOF) sobre substratos de Ti6Al4V. Los tamaños de partícula tanto de la titania como de la HA fueron similares para conseguir que las velocidades y temperaturas de las partículas durante el proceso de proyección fueran semejantes y las diferencias observadas en las propiedades de los recubrimientos se debieran únicamente a la diferente composición química y no a las condiciones de proyección. Para obtener las mismas condiciones de proyección para las diferentes mezclas, es decir temperatura y velocidad de partícula, fue necesario cambiar el caudal de propileno, ya que la conductividad térmica de la titania y de la HA es diferente. La difracción de rayos X no mostró la formación de nuevas fases por reacción química entre la $TiO_2$ y la HA. Debido a las propiedades mecánicas de la HA, su adición disminuyó la adherencia entre el substrato y el recubrimiento y los valores de dureza, especialmente cuando el contenido de HA fue del 20%; sin embargo, los valores de la adherencia fueron muy superiores a aquellos de se consiguen en recubrimientos únicamente de HA.

Es la primera vez que se obtiene este tipo de recubrimientos por proyección térmica. La adición de HA a recubrimientos de titania nanoestructurada podría combinar el buen funcionamiento mecánico y la estabilidad química de la titania y la bioactividad de la hidroxiapatita (HA).

ELSEVIER

Materials Science and Engineering A 458 (2007) 141–149

MATERIALS SCIENCE & ENGINEERING A

www.elsevier.com/locate/msea

# Nanostructured titania/hydroxyapatite composite coatings deposited by high velocity oxy-fuel (HVOF) spraying

M. Gaona [a], R.S. Lima [b,*], B.R. Marple [b]

[a] *Thermal Spray Centre, Universitat de Barcelona, Martí i Franquès 1, 08028 Barcelona, Spain*
[b] *National Research Council of Canada, 75 de Mortagne Blvd., Boucherville, QC J4B 6Y4, Canada*

Received 16 October 2006; received in revised form 8 December 2006; accepted 15 December 2006

**Abstract**

Pure nanostructured titania ($TiO_2$) and blends with 10 and 20 wt% hydroxyapatite (HA) powders were sprayed onto Ti–6Al–4V substrates using a high velocity oxy-fuel (HVOF) system. The feedstock powders employed in this work were engineered to exhibit similar particle size distributions in order to generate similar values of particle temperature and velocity in the spray jet. By achieving these characteristics it was assumed that the differences in coating properties and microstructures produced in this study were mainly related to the nature and composition of the feedstock powders, rather than to the spraying parameters or in-flight particle characteristics. The microstructure, porosity, roughness, Vickers hardness and bond strength (ASTM C633) of these coatings were analyzed and evaluated. X-ray diffraction (XRD) patterns showed that no detectable chemical reaction occurred between the nanostructured $TiO_2$ and HA phases during the spray process. Due to the poor mechanical performance of HA, its addition decreased the bond strength and hardness values of the coatings, especially when the content of HA was 20 wt%; however, the bond strength values were still much superior to those of HA thermally sprayed coatings. The addition of HA to nanostructured titania for producing HVOF-sprayed coatings could be very interesting for biomedical applications due to the combination of the good mechanical performance and chemical stability of nanostructured titania and a bioactive phase (HA) that can enhance the bio-performance of the coating.
Crown Copyright © 2007 Published by Elsevier B.V. All rights reserved.

*Keywords:* Thermal spray; High velocity oxy-fuel (HVOF); Nanostructured titania ($TiO_2$); Hydroxyapatite (HA); Titania-hydroxyapatite; Mechanical performance

## 1. Introduction

### 1.1. Hydroxyapatite thermal spray coatings

Hydroxyapatite (HA) has been extensively studied and clinically applied for its bioactive properties in medicine. HA is too brittle to be used as bulk material under loaded conditions, so HA is normally applied as a coating on metallic substrates in order to combine the mechanical strength of metals with the excellent biological properties of HA. Although HA coatings have been applied by a wide range of surface deposition techniques, the air plasma spray (APS) process is still the most commercially used technology and is a relatively efficient, fast and economic approach. During the spraying, the material is fully or partially melted in the plasma jet and sprayed at high velocities onto a substrate to build up the coating. However, due to the extremely high temperatures of the plasma jet and the rapid cooling rate of sprayed particles when impacting the substrate, the degradation of HA to other bioresorbable phases, such as tricalcium phosphate (α or β-TCP), tetracalcium phosphate (TTCP) or the non-biocompatible CaO is inevitable [1,2].

It has been pointed out that the use of HA-coated implants is often based on relatively short-term medical data that may not necessarily be an indicator of the long-term performance. Some authors have reported that the effects of disintegration of the HA coatings only become clinically evident after 5–6 years in HA-coated acetabular prostheses and that dissolution is accelerated on areas subjected to a high level of loading [3]. Studies involving analysis of the HA coating surface after implantation indicated dissolution, osteoclastic resorption, and carbonate apatite precipitation had occurred [4,5]. These are among the reasons why new biocompatible coatings with improved mechanical strength, chemical stability in the human

* Corresponding author. Tel.: +1 450 641 5150; fax: +1 450 641 5105.
*E-mail address:* rogerio.lima@cnrc-nrc.gc.ca (R.S. Lima).

0921-5093/$ – see front matter. Crown Copyright © 2007 Published by Elsevier B.V. All rights reserved.
doi:10.1016/j.msea.2006.12.090

body and even higher biocompatibility levels are being sought by various researchers.

### 1.2. Titania ($TiO_2$) as a biomedical coating

The use of titanium metal, considered to be bioinert, as an implant material is based on its load bearing properties and the good biocompatibility properties of its thin native oxide layer ($TiO_2$), which does not exhibit resorption by the human body fluids. These properties have led to titania being deposited onto metallic substrates for biomedical applications, although it is generally considered not as bioactive as HA.

It has been reported that high velocity oxy-fuel (HVOF) sprayed nanostructured titania coatings exhibit higher bond strength, higher crack propagation resistance and higher wear resistance compared to the conventional titania coatings [6,7]. It was hypothesized that the semi-molten nanostructured titania particles (nanozones), spread and embedded throughout the coating microstructure, were responsible for the good mechanical behavior, i.e., it was suggested that they acted as crack arresters, thereby improving coating toughness [6,7]. In addition to the good mechanical properties, the nanostructured titania coatings and bulk were shown to possess properties important for implantation; for example, a bonelike apatite formation on the surface of the coating after immersion in simulated body fluids, an osteoblast cell growth (in vitro) equivalent or superior to that of APS HA coatings, and an increase in osteoblast adhesion (cell cultures) compared to non-nanostructured materials [8–10]. It is believed that the nanostructured surface topography plays a significant role in the adsorption of ions and adhesion protein cells of the osteoblasts (vitronectin and fibronectin) [11,12].

HVOF-sprayed nanostructured $TiO_2$ coatings have demonstrated superior mechanical behaviour when compared to that of HA thermal spray coatings (APS or HVOF-sprayed) [13]. As previously stated, this type of $TiO_2$ coating exhibited an osteoblast cell growth (in vitro) equivalent or superior to that of APS HA coatings [9]. It is speculated that this "good" biological performance could be enhanced by the addition of HA in the coating composition.

The information available to the authors indicated that $TiO_2$ + HA mixtures have not been used in the production of implants on a commercial scale, however, it is possible to find different references in the literature about the use of $TiO_2$ + HA composites as biomedical materials. Li [14] produced $TiO_2$ and $TiO_2$ + 15 vol.% HA rods via hot isostatic pressing. These rods were implanted in the femurs of rabbits. After three months of implantation the rabbits were euthanized and push out tests were performed. The $TiO_2$ + 15 vol.% HA composite rods showed an increase of shear strength of 1.7 times when compared to that of the pure $TiO_2$ rods. Ramires et al. [15] studied the biocompatibility (in vitro) of $TiO_2$ + HA coatings prepared via sol–gel. The results demonstrated that the $TiO_2$ + HA coatings were not cytotoxic and allowed the proliferation of human osteoblast-like cells. The bioactivity of the $TiO_2$ + HA coatings was the result of the presence of hydroxyl groups detected on their surfaces, which promoted calcium and phosphate precipitation, improving the interactions with the osteoblast cells. These references confirm that $TiO_2$ + HA mixtures have potential as biomaterials.

The objective of this work was to HVOF spray nanostructured $TiO_2$, nanostructured $TiO_2$ + 10 wt% HA and nanostructured $TiO_2$ + 20 wt% HA feedstock powders, in order to engineer coatings having the good mechanical performance of the HVOF-sprayed nanostructured titania and the proven biocompatibility of HA. In order to try to separate the effects of powder composition and morphology on the microstructure and mechanical performance of the coatings from that of the in-flight characteristics of the particles during thermal spraying, the feedstock powders were engineered to exhibit a similar particle size distribution and were thermally sprayed by choosing spray parameters that produced similar values of particle temperature and velocity in the HVOF jet. Using this processing approach it was assumed that any differences in mechanical performance and microstructure observed among the three coatings would be mainly related to the composition/morphology of the powders, and not the in-flight particle characteristics, i.e., particle temperature and velocity.

## 2. Experimental procedure

### 2.1. Feedstock powders

The feedstock powder mixtures were composed of 80 wt% nano $TiO_2$–20 wt% HA, 90 wt% nano $TiO_2$–10 wt% HA and pure nanostructured titania. The starting nanostructured titania feedstock (VHP-DCS (5–20 μm), Altair Nanomaterials Inc., Reno, NV, USA) had a nominal particle size distribution from 5 to 22 μm. The HA powder (Captal 30 SD, Plasma Biotal, UK) was pure and highly crystalline and was sieved to produce particles with diameters smaller than 22 μm to ensure the uniformity of the mixture with titania. The feedstock powders were prepared through a mechanical-blending process in a planetary mill (P5, Fritsch GmbH, Germany). Powder particle size distribution was performed by a laser diffraction particle size analyzer (Beckman Coulter LS 13320, Beckman Coulter, Miami, FL, USA).

### 2.2. Thermal spraying and in-flight particle diagnostics

The three feedstock powders were thermally sprayed via the HVOF technique using an oxy-propylene based HVOF torch (Diamond Jet 2700-hybrid, Sulzer Metco, Westbury, NY, USA). The coatings were deposited onto Ti–6Al–4V substrates that had been grit-blasted before spraying.

Particle diagnostics were performed in order to evaluate in-flight particle properties. For this purpose, an in-flight diagnostic tool (DPV 2000, Tecnar Automation, Saint Bruno, QC, Canada) was employed. This system uses infrared pyrometry in order to perform the in-flight diagnostics on 5000 sprayed particles.

Different propylene flow rates were tested by monitoring particle temperature and velocity. The parameter sets selected for coating production were the ones that produced similar values for average particle temperature (∼30 °C above the melting point of titania) and velocity in the thermal spray jet for the three different feedstock powders. The measurements were performed

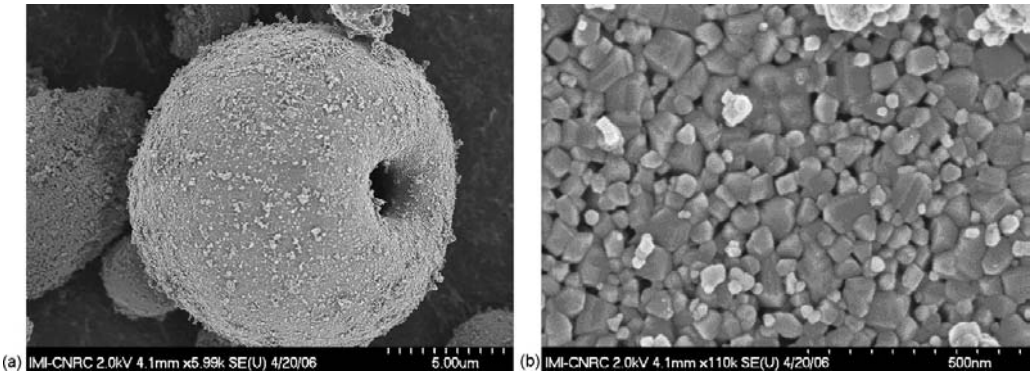


Fig. 1. (a) Morphology of spray-dried titania feedstock particle. (b) Particle of (a) observed at higher magnification—individual nanosized titania particles.

from the centerline of the HVOF jet at the standoff distance for coating deposition (20 cm).

Moreover, during the spraying process the substrate temperature was recorded using a pyrometer. In order to reduce the coating temperature, a cooling system (air-jets) was used and the temperature was kept below 170 °C for all the coatings.

### 2.3. Structure and phase characterization

Powder morphology, surface topography and cross-sections of the coatings were examined using field emission scanning electron microscopy (FE-SEM). Samples were cut with a diamond saw, vacuum impregnated with a low viscosity epoxy resin (Caldo Fix, Struers, USA) and, finally, polished using standard metallographic procedures. Ten images of the cross-section of each coating were analyzed via image analysis in order to determine the porosity levels.

The phases present in both the starting powder and the coatings were determined by means of X-ray diffraction (XRD) using Cu Kα radiation and a scan speed of 0.05° for values of $2\theta$ between 20° and 60°.

Roughness and surface topography are important parameters in biocompatible coatings [16,17]. Roughness measurements of the HVOF coatings were carried out by two different techniques: (i) tactile roughness tester (profilometer Mitutoyo Surftest 301, Mitutoyo, Japan) and (ii) confocal microscopy, which is a non-contact optical imaging profiler (PLu 2300 Optical Profiler, Sensofar-Tech, SL, Barcelona, Spain). In the latter case, roughness profiles were obtained by filtering the roughness effects for which the wavelength was superior to the selected cut-off length ($\lambda_c$). A cut-off value of 0.800 mm was selected, using a filter of Gaussian type as recommended by the norm ISO 11562:1996 [18]. For each technique, 10 measurements were carried out at various positions on the surface, then the coefficient of variance, the average and the standard deviation were calculated.

### 2.4. Mechanical properties

Vickers microhardness measurements (Micromet II, Buehler, Lake Bluff, IL, USA) were performed under a 300 g load for 15 s on the polished cross-section of the coatings. A total of 30 microhardness measurements were carried out for each coating in order to achieve a constant value of coefficient of variance (CV). It was necessary to adopt this procedure to ensure that there were enough statistical data to determine with precision the Weibull modulus distribution of the hardness values for each coating [19].

The bond strength of the coatings was tested using the ASTM standard C633-01 for determining the adhesion or cohesion strength of thermal spray coatings [20]. A total of five samples of each coating were employed, and the bond strength data was reported as the average value.

## 3. Results and discussion

### 3.1. Feedstock and particle size distribution

Fig. 1(a) shows the morphology of the nanostructured titania powders that were used in this work. It can be observed that the morphology of the spray dried titania feedstock was predominantly spherical, exhibiting the typical donut shape of spray dried particles. When analyzed at high magnification (Fig. 1b) it is possible to observe an agglomeration of titania nanoparticles smaller than 100 nm, indicating that the titania feedstock is nanostructured. The HA powder was also spray dried resulting in spherical particles (Fig. 2a). After the process of spray drying, the powders were sintered and densified (Fig. 2b) by the manufacturer. It can be observed that the internal structure of the HA particles is somewhat coarser than that of the $TiO_2$ particles.

Powder particle blends were observed after the mechanical mixing step. Fig. 3 shows a micrograph and the mapping spectra for the elements calcium and titanium in the nanostructured $TiO_2$ + 20 wt% HA powder system. It may be noted that the two constituents are relatively uniformly distributed in the mixture. Moreover, Fig. 4 shows the size distribution of the different feedstock powders, where it can be observed that the three feedstock powders exhibited similar particle size distributions.

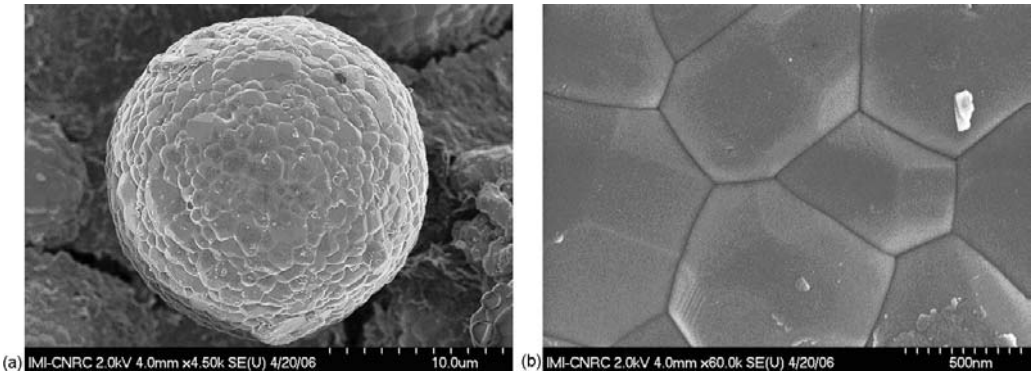


Fig. 2. (a) Morphology of spray-dried and sintered HA feedstock particle. (b) Particle of (a) observed at higher magnification—dense particle as a result of the sintering process.

### 3.2. In-flight particle characteristics

Fig. 5 shows the particle temperature and velocity distributions in the thermal spray jet for the three feedstock powders. The three sprayed powders showed similar distributions for the spraying parameters employed. Fig. 6 shows the histograms of particle diameter, temperature and velocity for the three spray parameters. It is possible to observe that the shapes of the distributions for the three spraying conditions are similar. The average particle temperature and velocity for the different spraying parameters are summarized in Table 1. That table shows that the average particle temperatures and velocities were in the range of 1874–1881 °C and 651–686 m/s. Therefore, the average particle temperature of all three spraying conditions was slightly above the melting point of titania (1855 °C) [21].

The thermal conductivity (K) of the titania and hydroxyapatite bulk materials are 7.4 and 1.25 W/mK, respectively [21], so titania is more able to conduct heat. Therefore more thermal energy is required for an HA particle to reach a given temperature level than needed for a $TiO_2$ particle. In fact, it was observed that during HVOF spraying it was necessary to use a higher propylene flow when spraying nanostructured $TiO_2$ + HA as compared to that required when spraying pure nanostructured $TiO_2$.

It is important to point out that the objective of HVOF spraying the three feedstock powders at similar levels and distributions of particle temperature and velocity was achieved. Therefore, it is assumed that the difference in results and characteristics of residual stress, microstructure, phase content and mechanical properties discussed in the next sections are mainly related to the composition of each feedstock, and not to the in-flight particle characteristics.

Table 1
HVOF average particle temperature and velocity for each system

| wt% HA | $T$ (°C) | $V$ (m/s) |
|---|---|---|
| 0 | 1881 ± 162 | 686 ± 93 |
| 10 | 1875 ± 135 | 651 ± 88 |
| 20 | 1874 ± 132 | 654 ± 91 |

### 3.3. Microstructural characterization of the coatings

Figs. 7–9 show the cross-section of the coatings. It is possible to observe that the nanostructured $TiO_2$ coating microstructure is relatively dense and homogeneous, not exhibiting the typical layered or lamellar structure of thermal spray coatings (Fig. 7). It may be assumed that this coating exhibits an isotropic "bulk-like" microstructure and low porosity (3%) due, in part, to the high particle velocity at the point of impact with the substrate (686 ± 93 m/s).

After spraying, the HA and $TiO_2$ phases were relatively homogeneously distributed in the coatings (Figs. 8 and 9). HA appears as lamellae in a titania matrix, but some spherical HA particles were also observed. The spherical particles represent HA particles that were slightly melted (outer shell) in the thermal spray jet. It is important to point out that HA has lower thermal diffusivity and conductivity values than those of titania. The porosity levels of the nanostructured $TiO_2$ + 10 wt% HA and nanostructured $TiO_2$ + 20 wt% HA coatings were less than 1%.

The as-sprayed top surfaces of the nanostructured $TiO_2$ + HA coatings are shown in Figs. 10 and 11. The surfaces were composed of titania and 20–30 μm diameter HA splats. This structure could be very interesting for biomedical applications due to the combination of the non-absorbable (stable) titania phase, and the bioactive HA phase.

The roughness values of the HVOF sprayed coatings measured by confocal microscopy and a contact tester are shown in Fig. 12. The same trend for the results was obtained for both techniques, although the roughness values and the standard deviation acquired by means of confocal microscopy were lower than those obtained by the roughness contact tester. The results indicated some increase of roughness with the hydroxyapatite content in titania coatings. The nanostructured $TiO_2$ + 20 wt% HA coating exhibited the highest roughness, which suggests that the roughness may be dominated by the HA splats since the topography of the titania is partially masked.

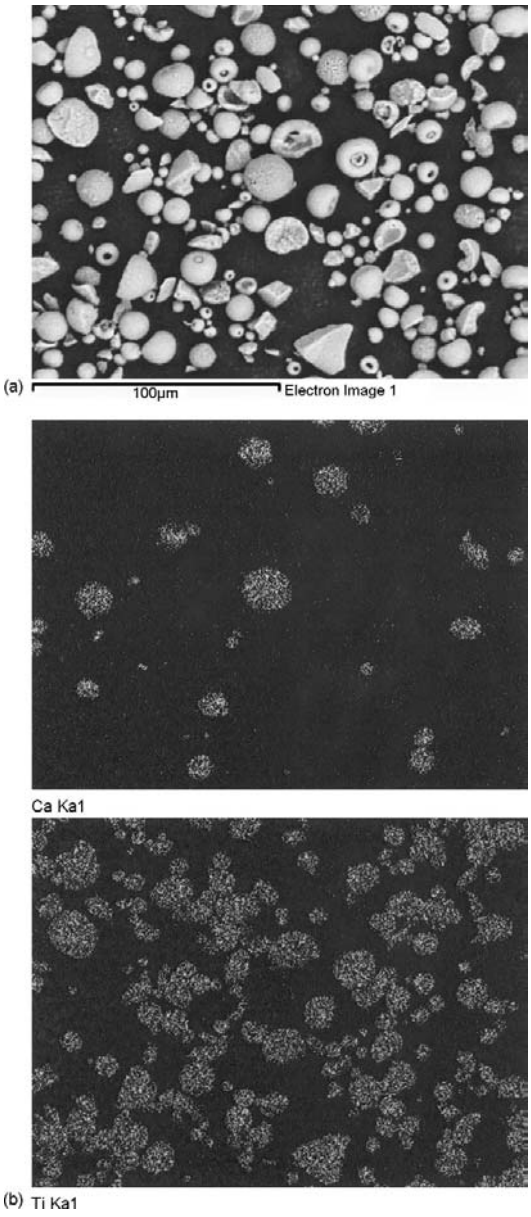


Fig. 3. Micrograph (a) and X-ray maps (b) showing Ca and Ti for the nanostructured titania + 20 wt% HA powder.

### 3.4. Phase content

The XRD patterns of the as-sprayed titania coating and the nanostructured feedstock powder are shown in Fig. 13. The volume percentage of anatase was determined according to the following equation [22]:

$$C_A = \frac{8I_A}{(13I_R + 8I_A)} \quad (1)$$

where $I_A$ and $I_R$ are the X-ray intensities of the anatase (1 0 1) and the rutile (1 1 0) peaks, respectively. It can be observed that a phase transformation occurred during the thermal spraying of titania. The starting powder was mainly composed of anatase (86%); and after spraying, the amount of anatase was reduced to 17%, with the main phase being rutile. Of the three polymorphic forms of titania, rutile is the only stable phase, whereas anatase and brookite are metastable and are transformed to rutile irreversibly by heating. The anatase-rutile transition has been reported to take place between 400 and 1000 °C, depending on the microstructure of the powders of anatase, the impurity content, deviations in the stoichiometry, superficial area and particle size [21]. The residual anatase phase present in the coating was probably the result of semi-molten nanostructured powder particles that were embedded in the coating microstructure. It is important to point out that these semi-molten nanostructured particles (nanozones) present in the coating are believed to be responsible for the good mechanical performance of the coating via the enhancement of its toughness [6,7].

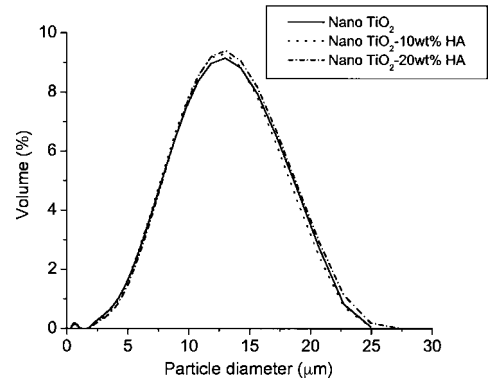


Fig. 4. Size distribution of the different powders sprayed.

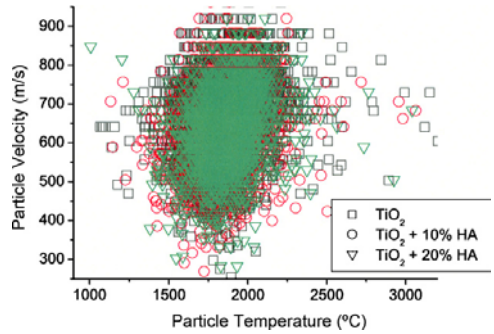


Fig. 5. Particle velocity vs. particle temperature for the three types HVOF-sprayed feedstock particles.

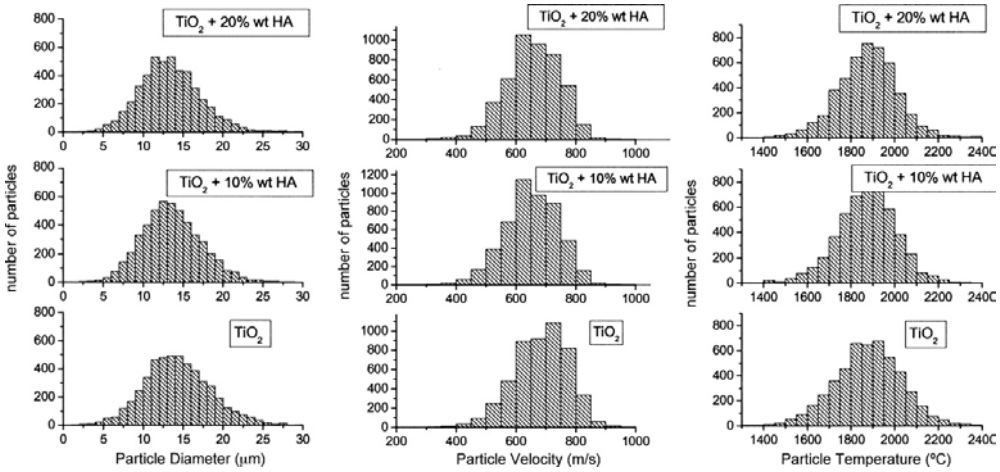


Fig. 6. Histograms of particle diameter, velocity and temperature for the three types of HVOF-sprayed feedstock particles.

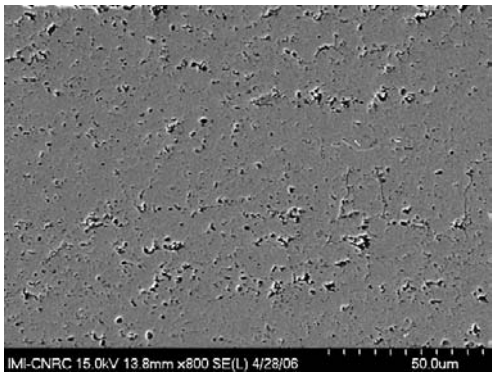


Fig. 7. Cross-section of the HVOF-sprayed nanostructured $TiO_2$ coating.

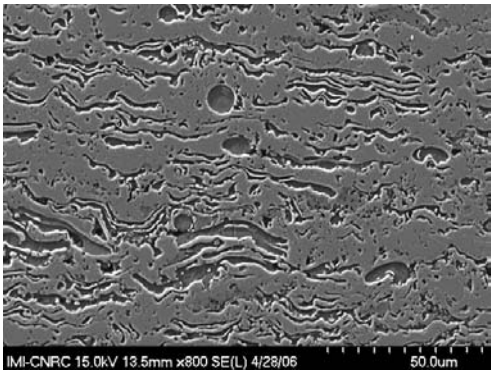


Fig. 9. Cross-section of the HVOF-sprayed nanostructured $TiO_2$ + 20 wt% coating.

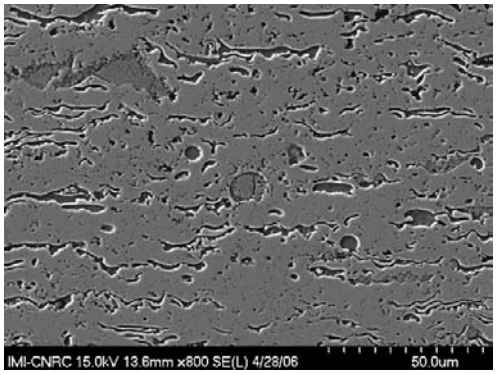


Fig. 8. Cross-section of the HVOF-sprayed nanostructured $TiO_2$ + 10 wt% HA coating.

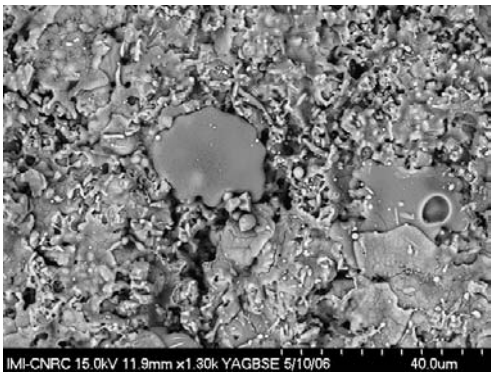


Fig. 10. As-sprayed top surface of the HVOF-sprayed nanostructured $TiO_2$ + 10 wt% HA coating.

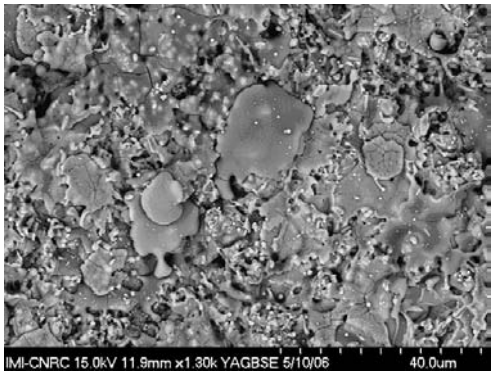


Fig. 11. As-sprayed top surface of the HVOF-sprayed nanostructured $TiO_2$ + 20 wt% HA coating.

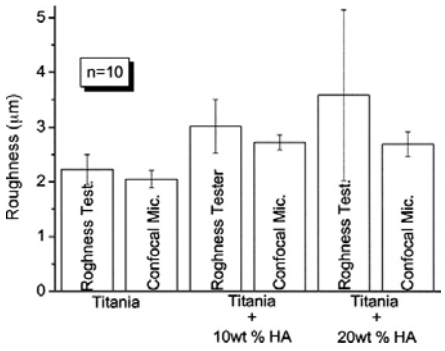


Fig. 12. Roughness values obtained for the different coatings and by two different techniques.

Figs. 14 and 15 show the patterns of the nanostructured $TiO_2$ + HA systems. These compositions exhibited transformations similar to the titania coating: the rutile peak intensity increased considerably after spraying, but the anatase peak intensity decreased. The feedstock powders and coatings were mainly composed of HA (JCPDS 9-432), rutile (JCPDS 21-1276) and anatase (JCPDS 21-1272) [23]. No tricalcium, tetracalcium phosphate or CaO often produced due to the thermal decomposition of HA were detected by XRD. The reasons why other calcium phosphate phases were not detected in the coatings may be related to the fact that titania was the main phase and may have masked the XRD peaks of other calcium phosphate phases if they were formed in small amounts [24]. Moreover, no chemical products resulting from the reaction between HA and $TiO_2$ were observed following the spraying. The absence of such evidence in the XRD spectra was probably caused by the (i) fact the powders were blended (i.e., not intimately mixed) and (ii) short time that the particles were in the HVOF jet [25].

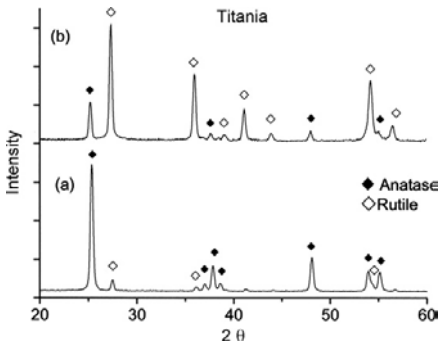


Fig. 13. XRD patterns of the nanostructured $TiO_2$ feedstock (a) and HVOF-sprayed coating (b).

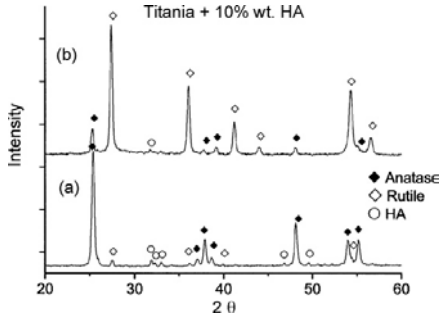


Fig. 14. XRD patterns of the nanostructured $TiO_2$ + 10 wt% HA feedstock (a) and HVOF-sprayed coating (b).

### 3.5. Hardness and Weibull modulus

Fig. 16 shows the Vickers hardness values (300 g load) obtained for the cross section of the HVOF coatings. The coefficient of variation (CV) for the hardness measurements on each sample stabilized around 20 measurements and, therefore, 30 microhardness measurements were taken for each sample. As expected, the hardness values were decreased by the addition of HA.

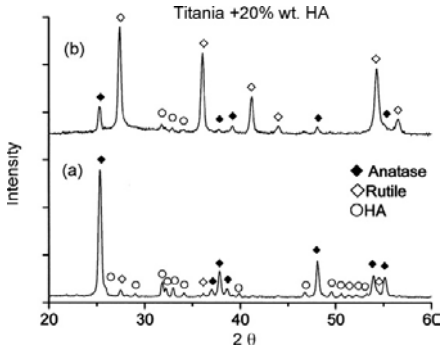


Fig. 15. XRD patterns of the nanostructured $TiO_2$ + 20 wt% HA feedstock (a) and HVOF-sprayed coating (b).

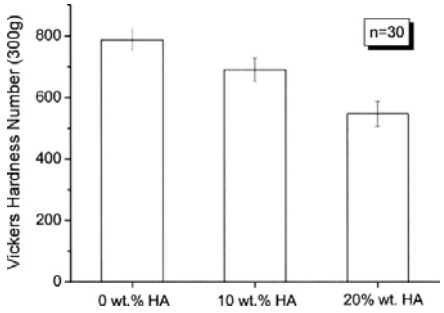


Fig. 16. Vickers hardness of the HVOF-sprayed coatings.

Fig. 17 shows the Weibull modulus distribution of the hardness on the cross-section of the three HVOF coatings. The Weibull modulus measures the variability of the mechanical properties of ceramic materials. According to Weibull theory, the cumulative probability that a sample will yield at a particular random property value ($x_i$) is $P_i$:

$$P_i = 1 - \exp\left[-\left(\frac{x_i - x_u}{x_0}\right)^m\right] \quad (2)$$

where $x_0$ is a normalizing constant that represents the characteristic value below which 63.2% of the data lie, $x_u$ the threshold value below which there is no failure, and $m$ is the Weibull modulus which defines the shape of the distribution.

A more useful determination of the Weibull modulus is to estimate the probability of yield at a particular value for each sample as $P_i = i/(N+1)$. One first ranks the samples in order of increasing mechanical property value and assigns an index $i = 1$ for the lowest value $x_1$, $i = 2$ for the second lowest value $x_2$, and so on, up to $i = N$ for the highest value of mechanical property $x_N$. Then the data is finally plotted in the following linearized form of the Weibull distribution:

$$\ln\left[\ln\left(\frac{1}{1-P_i}\right)\right] = m\ \ln\ x_u - m\ \ln\ x_0 \quad (3)$$

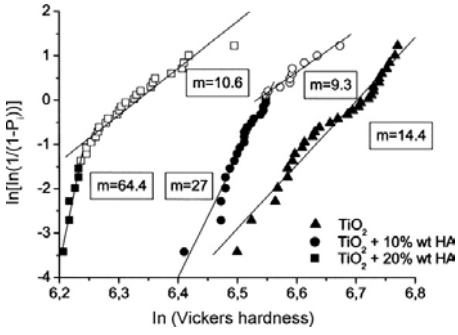


Fig. 17. Weibull modulus distributions of the Vickers hardness of the HVOF-sprayed nanostructured $TiO_2$ and the two nanostructured $TiO_2$ + HA coatings.

Table 2
Weibull modulus values of the Vickers hardness of the HVOF-sprayed coatings

| System (wt% HA) | Weibull modulus | |
|---|---|---|
| 0 | 14.4 | |
| 10 | 9.3 | 27 |
| 20 | 10.6 | 64.4 |

where Weibull modulus, $m$, is the slope of the $\ln[\ln(1/(1-P_i))]$ versus $\ln x_u$ plot [26]. The values of the Weibull modulus are summarized in Table 2.

The Vickers hardness Weibull plot of the titania coating exhibits a linear behaviour indicative of the homogenous coating structure (Fig. 17). A Weibull modulus of 14.4 was found for this coating. However, the Weibull modulus plots of the titania-HA coatings exhibit a bimodal distribution. In order to determine the exact point where the slopes of the bimodal coatings (nanostructured $TiO_2$ + 10 wt% HA and nanostructured $TiO_2$ + 20 wt% HA) are localized in Fig. 17, the $r^2$ statistics were determined with respect to the number of measurements. The $r^2$ factor was plotted for 3, 4, 5, etc. measurements of $\ln[\ln(1/(1-P))]$ until all the 30 measurements were taken into account. For each one of the bimodal coatings, there was a point where the $r^2$ maximum was achieved (peak). This data value corresponds to a transition point between the two distributions [27]. It should be pointed out that the Vickers hardness impressions in the nanostructured $TiO_2$ + HA coatings exhibited diagonal lengths on the order of 25–35 μm. As thermally sprayed splats normally exhibit thicknesses around 1 μm or of just a few microns, and by observing the scale of features in the coating microstructures (Figs. 8 and 9), it can be assumed that each indentation sampled both nanostructured $TiO_2$ and HA phases at the same time, i.e., individual phases (regions) of $TiO_2$ and HA were probably not sampled. However, probably there were regions in the microstructure of the coatings where the $TiO_2$–HA mixture was more homogeneous than others. Therefore, the regions exhibiting higher homogeneity would probably present higher Weibull modulus values (less data scattering) than those regions with lower degree of $TiO_2$–HA homogeneity, thereby giving rise to the bimodal distribution. It is important to point out that for the bimodal coatings, the upper slope of the Weibull moduli distributions exhibit a similar value (~9 to 11). It is also observed that as the HA content increases from 10 to 20%, the length of the upper slope increases and the lower slope tends to be minimized. From this observation, it can be inferred that if the HA content is increased to values higher than 20 wt%, the bimodal distribution will probably tend to disappear. This would occur because the degree of mixing of both phases ($TiO_2$ and HA) would become more uniform for higher amounts of HA. The distribution of both phases would tend to become so homogeneous, that a linear distribution would be observed.

### 3.6. Bond strength

Nanostructured titania and nanostructured $TiO_2$ + 10 wt%. HA coatings failed at the epoxy glue during bond strength testing (ASTM C633). Because these samples had a glue failure, the

exact bond strength of these thermal spray coatings could not be quantified. The strength of the epoxy glue was previously tested and indicated a value of 77 MPA (∼11,000 psi), therefore, the bond strength of the nanostructured titania and nanostructured $TiO_2$ + 10 wt% HA coatings was higher than this value. However, the nanostructured $TiO_2$ + 20 wt% HA coatings showed an adhesive-cohesive failure and an adhesion value of 68 ± 14 MPa, which demonstrates that the addition of HA weakened the bond strength of the HVOF-sprayed nanostructured titania coating. This lower value could be attributed to the weak mechanical bonding between HA and titania splats, where apparently no chemical reaction occurred, and to the known low mechanical performance of HA. It is important to point out that this value (68 ± 14 MPa) is higher than those generally found in the literature for thermal spray HA coatings (e.g., 31 MPa) [28] or HVOF-sprayed conventional $TiO_2$ + HA coatings (e.g., 28 MPa) [24].

## 4. Conclusions

In this work, nanostructured $TiO_2$, nanostructured $TiO_2$ + 10 wt% HA and nanostructured $TiO_2$ + 20 wt% HA were HVOF sprayed with powders having similar particle size distributions and similar distributions of the in-flight particle characteristics (i.e., temperature and velocity). Because of this approach, it is believed that differences of microstructure and properties of the engineered coatings observed in this work were mainly related to the powder morphology and composition, rather than to the differences in particle temperature and velocity.The majority of the anatase phase of nanostructured $TiO_2$ powder transformed to rutile during HVOF spraying. The anatase phase observed in the coatings was probably the result of semi-molten nanostructured $TiO_2$ particles embedded in the coating microstructure. For the coatings produced from the mixture of nanostructured $TiO_2$ + HA powders, it was observed that (i) the phases were relatively homogeneously distributed in the coating microstructure and (ii) no significant chemical reaction occurred between the two constituents ($TiO_2$ and HA) of the sprayed powders. In addition, no significant HA degradation was observed by means of XRD.The Vickers hardness results and the adhesion tests showed that the addition of HA weakened the mechanical properties of the titania coatings, however, the bond strength values obtained were higher than those generally found in the literature for thermally sprayed HA coatings.The nanostructured $TiO_2$ + HA coatings tended to exhibit the highest values of roughness, which suggests that the roughness may be dominated by the HA splats since the topography of the titania tends to be masked by the HA particles. As HA is a bioactive material, this surface characteristic found in this study is probably very interesting for biomedical applications.A bimodal Weibull distribution was observed for the hardness values of the nanostructured titania + HA coatings. This bimodal distribution tends to disappear as the HA content increases, as an indicator of the homogeneity of the phase distribution, i.e., the two phases tend to be well-distributed throughout the coating microstructure.The HVOF-sprayed nanostructured titania + HA coatings may become a very interesting alternative for biomedical applications due to the combination of a high mechanical performance and non-absorbable nanostructured $TiO_2$ phase (stable), and a bioactive HA phase, that can enhance the bio-performance of the coating.

## Acknowledgements

The authors thank J.-F. Alarie for metallography and adhesion testing, F. Belval for HVOF spraying, M. Lamontagne for in-flight particle diagnostics and M. Thibodeau for SEM observations. Moreover, M. Gaona thanks the Generalitat de Catalunya (Spain) for the Formació de Personal Investigador (FI) grant and the Thermal Spray Centre for the financial support.

## References

[1] P. Cheang, K.A. Khor, Biomaterials 17 (1996) 537–544.
[2] L. Sun, C.C. Berndt, C.P. Grey, Mater. Sci. Eng. A. 360 (2003) 70–84.
[3] M.T. Manley, W.N. Capello, J.A. D'Antonio, A.A. Edidin, R.G.T. Geesink, J. Bone Joint Surg. 80A (1998) 1175–1185.
[4] O. Reikeras, R.B. Gunderson, Acta Orthop. Scand. 73 (2002) 104–108.
[5] K.A. Gross, W. Walsh, E. Swarts, J. Therm. Spray Technol. 13 (2004) 190–197.
[6] R.S. Lima, B.R. Marple, Mater. Sci. Eng. A 395 (2005) 269–280.
[7] R.S. Lima, B.R. Marple, Surf. Coat. Technol. 200 (2006) 3428–3437.
[8] J. Shi, C. Ding, Y. Wu, Surf. Coat. Technol. 137 (2001) 97–103.
[9] J.-G. Legoux, F. Chellat, R.S. Lima, H. Shen, B.R. Marple, M.N. Bureau, G.A. Candeliere, J. Therm. Spray Technol., in press.
[10] L.G. Gutwein, T.J. Webster, Biomaterials 25 (2004) 4175–4183.
[11] T.J. Webster, C. Ergun, R.H. Doremus, R.W. Siegel, R. Bizios, J. Biomed. Mater. Res. 51 (2000) 475–483.
[12] R. Rohanizadeh, M. Al-Sadeq, R.Z. LeGeros, J. Biomed. Mater. Res,. 71 (2004) 343–352.
[13] R.S. Lima, H. Li, K.A. Khor, B.R. Marple, J. Therm. Spray Technol., in press.
[14] J. Li, Biomaterials 14 (3) (1993) 229–232.
[15] P.A. Ramires, A. Romito, F. Cosentino, E. Milella, Biomaterials 22 (2001) 1467–1474.
[16] G. Lauer, M. Wiedmann-Al-Ahmad, J.E. Otten, U. Hübner, R. Schmelzeisen, W. Schilli, Biomaterials 22 (2001) 2799–2809.
[17] K. Cai, J. Bossert, K.D. Jandt, Colloids Surf. B: Biointerfaces 49 (2006) 136–144.
[18] Geometrical Product Specifications (GPS), Surface texture: profile method—metrological characteristics of phase correct filters. Standard ISO 11562:1996 -International Organization for Standardization.
[19] C.K. Lin, C.C. Lin, C.C. Berndt, J. Am. Ceram. Soc. 78 (1995) 1406–1410.
[20] Standard Test Method for Adhesion or Cohesion of Thermal Spray Coatings, ASTM Standard C 633-01. ASTM, West Conshohocken, PA, USA.
[21] M. Miyayama, K. Koumoto, H. Yanagida:, Engineering properties of single oxides, in: S.J. Schneider (Ed.), Engineered materials handbook, 4-ceramic and glasses, ASM International, Materials Park, OH, 1991, pp. 748–757.
[22] N. Berger-Keller, G. Bertrand, C. Filiatre, C. Meunier, C. Coddet, Surf. Coat. Technol. 168 (2003) 281–290.
[23] Powder Diffraction File Alphabetic PDF-2 Data Base, file 9-432, 21-1276 and 21-1272. International center of diffraction Data, Newton Square, PA, USA, 1994.
[24] H. Li, K.A. Khor, P. Cheang, Biomaterials 23 (2002) 85–91.
[25] J. Weng, X. Liu, X. Zhang, X. Ji, J. Mater. Sci. Lett. 13 (1994) 159–161.
[26] R.S. Lima, B.R. Marple, J. Therm. Spray Technol. 12 (2003) 360–369.
[27] R.S. Lima, A. Kucuk, C.C. Berndt, Mater. Sci. Eng. A. 327 (2002) 224–232.
[28] H. Li, K.A. Khor, P. Cheang, Mater. Sci. Eng. A. 293 (2000) 71–80.

## 8.4 Discusión de resultados

La microestructura de los recubrimientos obtenidos es densa y homogénea y no se observan ni grietas ni la típica estructura laminar de los recubrimientos de proyección. Se podría asumir que estos recubrimientos son casi homogéneos con baja porosidad debido a la alta velocidad de las partículas que presentan las partículas cuando impactan contra el substrato. A medida que aumenta la velocidad y la temperatura de las partículas el recubrimiento se vuelve más homogéneo y más tensionado a compresión.

La composición de los recubrimientos está fuertemente relacionada con las condiciones de proyección. A pesar que la anatasa es la fase prioritaria en el polvo de partida, la fase prioritaria en los recubrimientos es rutilo. La anatasa es una fase metaestable que transforma irreversiblemente a rutilo a 400-1000ºC. Parte de la anatasa del polvo original queda retenida en los recubrimientos debido al rápido enfriamiento de las partículas durante el proceso de proyección.

Los valores de dureza vickers también aumentaron a medida que la velocidad de las partículas aumentaba. Es decir, los recubrimientos menos porosos son los que tienen más dureza y de módulo de weibull más elevado. Comparando con otros recubrimientos de proyección térmica los que se han estudiado tienen un modulo de weibull mayor. Este análisis cuantifica el comportamiento del material en cuanto a su variabilidad en propiedades mecánicas.

En el caso de los recubrimientos que se obtuvieron a partir de mezclas de titania y HA fueron relativamente densos y con los dos materiales homogéneamente distribuidos. A medida que aumentaba el contenido en HA aumentaba la rugosidad ya que los splats de HA enmascaraban la nanorugosidad de la titania. La fase predominante del polvo de titania fue anatasa, pero después de la proyección se

obtuvo mayoritariamente rutilo que es la fase estable de la titania. La anatasa residual probablemente procede de partículas semifundidas que han retenido su fase inicial. No se observaron, mediante difracción de rayos X, otras fases resultantes de la descomposición de la HA como son el alfa, beta-TCP, el TTCP o el CaO. El motivo podría ser que los picos de estas fases quedan enmascarados por los de la titania al ser la fase mayoritaria. Tampoco se encontraron productos de reacción entre la HA y la titania. Este hecho se podría deber a que los polvos no estaban mezclados íntimamente o que el tiempo de las partículas en el haz de proyección es tan corto que no pueden reaccionar entre sí.

El modulo de weibull de los recubrimientos de titania es lineal, mientras que los de HA + titania presentan un comportamiento bimodal. En los gráficos existe una pendiente con un valor de 9-11 que aumenta de longitud a medida que aumenta el contenido en HA. Este módulo de weibull se refiere a la homogeneidad del recubrimiento.

Los recubrimientos con el 0% y el 10% de HA rompieron por el pegamento durante el ensayo de adherencia, por lo que su valor de adherencia es superior a 77 MPa. Por el contrario al aumentar el contenido de HA al 20% el recubrimiento presento un fallo adhesivo-cohesivo con un valor de 68 ± 14 MPa. Esto se debe a la débil unión mecánica entre la HA y la titania. A pesar de ello este valor es superior a los de HA.

Se ha empezado a estudiar la citotoxicidad en este tipo de recubrimientos [12, 13] . Se cree que la biocompatibilidad se podría acentuar por la presencia del carácter nanoestructural de la superficie junto a una mejora del funcionamiento mecánico de estos recubrimientos.

Uno de los retos de los próximos años será probablemente la producción de recubrimientos biomédicos, mediante proyección térmica u otras tecnologías, que

exhiban características superficiales nanoestructurales con el fin de producir superficies biomiméticas. Es importante precisar de nuevo que la idea de combinar el funcionamiento mecánico de los recubrimientos nanoestructurados obtenidos por proyección térmica y la mejora de la biocompatibilidad es nueva y por lo tanto es necesario seguir investigando. De hecho, esto es un campo abierto con muchas posibilidades y oportunidades para el desarrollo y el uso.

## 8.5 Conclusiones del capítulo

- Los recubrimientos de titania obtenidos por proyección térmica de alta velocidad (HVOF) presentan una microestructura uniforme y una baja porosidad.

- Las fases presentes en los recubrimientos dependen considerablemente de las condiciones de proyección. Aunque la anatasa fuera la fase predominante en los polvos de partida, después de la proyección los recubrimientos están formados, principalmente, por rutilo con una proporción menor de anatasa. El contenido de anatasa en los recubrimientos tiende a aumentar con la temperatura y la velocidad de partícula.

- La adición de HA a los recubrimientos de titania debilita las propiedades mecánicas, sin embargo, los valores de adherencia obtenidos fueron más elevados que los observados para los recubrimientos de HA.

- Se ha observado una distribución bimodal de Weibull para los valores de dureza de los recubrimientos de titania nanoestructurada + HA. Esta distribución bimodal tiende a desaparecer con el aumento del contenido de HA, como un indicador de la homogeneidad de la distribución de las fases.

- Ambos trabajos contribuyen a aumentar el conocimiento de las condiciones necesarias para conseguir recubrimientos casi isotrópicos de titania nanoestructurada por HVOF con buenas propiedades mecánicas. Estos recubrimientos pueden contribuir en la ingeniería biomédica debido a la combinación de propiedades mecánicas mejoradas con buena biocompatibilidad debido a la nanotopografía superficial. En especial, los recubrimientos de titania nanoestructurada + HA pueden ser una alternativa

muy interesante en aplicaciones biomédicas debido a la combinación del buen comportamiento mecánico, la estabilidad en medio fisiológico y la superficie nanoestructurada de la titania, así como la bioactividad que le confiere la hidroxiapatita.

- A pesar de las buenas propiedades mecánicas que presentan estos recubrimientos, es necesario realizar ensayos sobre su estabilidad en medios fisiológicos y su citotoxicidad para afirmar que estos recubrimientos pueden ser una alternativa a los de HA.

## 8.6 Referencias

1. S. Areva, H. Paldan, T. Peltola, T. Närhi, M. Jokinen, M. Lindén. Use of sol–gel-derived titania coating for direct soft tissue attachment. J. Biomed. Mater. Res. 70A, (2004), 169-178.

2. D. B. Haddow, J. M. Kelly, P. F. James, R. D. Short, A. M. Scutt, R. Rawsterne, S. Kotha. Cell response to sol–gel derived titania coatings. J. Mater. Chem. 10, (2000), 2795–2801.

3. T. J. Webster, R. W. Siegel, R. Bizios. Osteoblast Adhesion on Nanophase Ceramics. Biomaterials. 20, (1999), 1221-1227.

4. T. J. Webster, C. Ergun, R. H. Doremus, R. W. Siegel, R. Bizios. Enhanced Functions of Osteoblasts on Nanophase Ceramics. Biomaterials. 21, (2000), 1803-1810.

5.T. J. Webster, J.U. Ejiofor. Increased Osteoblast Adhesion on Nanophase Metals: Ti, Ti6Al4V, and CoCrMo. Biomaterials. 25, (2004), 4731-4739.

6. L. G. Gutwein, T. J. Webster. Increased Viable Osteoblast Density in the Presence of Nanophase Compared to Conventional Alumina and Titania Particles. Biomaterials. 25, (2004), 4175-4183.

7. T. J. Webster, C. Ergun, R. H. Doremus, R. W. Siegel, R. Bizios. Specific Proteins Mediate Enhanced Osteoblast Adhesion on Nanophase Ceramics. J. Biomed. Mater. Res. 51(3), (2000), 475-483.

8. K. Anselmo. Osteoblast Adhesion on Biomaterials. Biomaterials. 21, (2000), 667-681.

9. M. J. Dalby, M. O. Riehle, H. Johnstone, S. Affrossman, A. S. G. Curtis. Investigating the limits of filopodial sensing: a brief report using SEM to image the interaction between 10 nm high nano-topography and fibroblast filopodia. Cell Biol. Inter. 28, (2004), 229–236.

10. M. Gell, E. H. Jordan, Y. H. Sohn, D. Goberman, L. Shaw, T. D. Xiao. Development and implementation of plasma sprayed nanostructured ceramic coatings. Surf. Coat. Techn.146-147, (2001), 48-54.

11. H. Luo, D. Goberman, L. Shaw, M. Gell, Indentation fracture behavior of plasma-sprayed nanostructured Al2O3–13wt.%TiO2 coatings Mater. Sci. Eng. A. 346, (2003), 237–245.

12. J. G. Legoux, F. Chellat, R. S. Lima, B. R. Marple, M. N. Bureau, H. Shen, G. A. Candeliere. Development of osteoblast colonies on New Bioactive Coatings. Building on 100 years of success: Proceedings of the International Thermal Spray Conference 2006, Ed. B. R. Marple, M. M. Hyland, Y. C. Lau, R. S. Lima, J. Voyer, May 15-18, 2006. Seattle, WA, USA. ASM International; 2006.

13. B. R. Marple, R. S. Lima, H. Li, K. A. Khor. Biomimetic ceramic surfaces produced by thermal spraying nanostructured titania: A coating alternative to hydroxyapatite on orthopedic implants.? Key Eng. Mater. 309-311, (2006), 739-742.